Eidgenössische Technische Hochschule Zürich
Swiss Federal Institute of Technology Zurich

Empa
Materials Science and Technology

Mechanical Behaviour of Additively Manufactured Ti-6Al-4V Lattices for Biomedical Implants

Master's Thesis

Mickey Fürer

April, 2020

Advisors: Prof. Dr. E. Mazza, Dr. E. Hosseini

Department of Mechanical and Process Engineering, ETH Zürich
306 - Experimental Continuum Mechanics, Empa

Abstract

Additive manufacturing (AM) enables enormous possibilities in the area of biomedical implants. The main advantages of AM are design freedom for complex geometries regarding a few rules, possibility of manufacturing lightweight and tunable structures (lattices) and customizing parts without significant raise in costs. Using lattice structures for biomedical implants reduces the risk of stress shielding and offers the possibility for bone ingrowth. In this project the goal was to create a good basis for further studies by working on two specific topics: a constitutive model for AM Ti-6Al-4V and mechanical testing of lattice samples.

Strut test data and models were used to optimize material model parameters of AM Ti-6Al-4V. For the mechanical testing lattice samples manufactured with selective laser melting (SLM) with loading axis parallel to the printing plane (horizontally printed) were used. The lattices were differently treated before testing. One group of raw lattices, meaning no postprocessing, another group was etched with Kroll's reagent and a third was filled with an epoxy. Both tensile and fatigue testes were performed on all lattice types.

The constitutive model predicted an accurate value at maximum force for the lattices but overestimated the elastic behaviour. Regarding the tensile tests the strength of the etched samples was around 10% lower compared to the raw lattices, the epoxy filled 30% higher than the raw. The fatigue endurance behaviour of the etched lattices was comparable to the raw even if the struts were 25% thinner due to etching. The fatigue endurance performance of the epoxy filled lattices was around 10 times higher than the raw samples.

Due to smoother surface and therefore less notch effect the etched lattices could compensate the thinner struts. The effect of the epoxy in the lattices had a larger effect than expected. It is not only increasing the stiffness and strength by adding material, but also by restraining the freedom of movement of the struts of the lattice. Further studies with more samples are needed to confirm those results.

Acknowledgements

First of all I want to thank Prof. Dr. Edoardo Mazza for the opportunity to write my Master's Thesis in the Experimantal Continuum Laboratory.

Many thanks to Dr. Ehsan Hosseini for his supervision during this project. He was a big support, helped with tasks I was struggling with, kept always the overview over the project and reminded me of tasks which may have been forgotten. It was always interesting and a big pleasure to work with him.

Freddy Bürki for his help and advice in mechanical questions and for providing me his private vacuum pump and chamber.

To all people of the Experimantal Continuum Laboratory also a special thanks for their support and constructive cooperation.

Another thanks goes to the X-Ray Center at Empa, especially Dr. Thomas Lüthi, who helped us with the CT Scans and Christian Affolter from the Mechanical Systems Engineering group for his support with the postprocessing of the CT Data. Wandong Wang from the Structural Engineering Lab for his help and support with the epoxy.

To my predecessor and friend Serjosha Robmann, who introduced me to the project, helped me to start efficiently and was always available for questions I want also express my special thanks.

And last but not least I want to say thank you to my family and friends, who supported me during the last six months.

Contents

Contents **iii**

1 Introduction **1**
1.1 Motivation 1
1.2 Initial Situation and Objectives 2

2 Materials and Methods **5**
2.1 Constitutive Model for AM Ti-6Al-4V Lattices 5
2.1.1 Setup 5
2.1.2 Experimental Data Preparation 6
2.1.3 Material Parameter Optimization 6
2.2 Lattice Model 10
2.3 Experiments 11
2.3.1 Test Setup 11
2.3.2 Material 12
2.3.3 Simulation 13
2.3.4 Expectations 15

3 Results **17**
3.1 Constitutive Model for AM Ti-6Al-4V Lattices 17
3.1.1 Material Optimization 17
3.2 Experimental Results 20
3.2.1 Tensile tests 20
3.2.2 Fatigue tests 23

4 Discussion **27**
4.1 Constitutive Model for AM Ti-6Al-4V Lattices 27
4.2 Experiments 28
4.2.1 Tensile tests 28
4.2.2 Fatigue tests 29

5 Outlook **31**
5.1 Simulation 31
5.2 Experiments 32

List of Figures **33**

List of Tables **35**

Bibliography **37**

A Data Sheet Epoxy **41**

B Material Data Ti-6Al-4V Powder **45**

C Camera Specifications **49**

D Lens Specifications **51**

Chapter 1

Introduction

1.1 Motivation

Additive manufacturing (AM) is a manufacturing process with enormous potential. Big improvement over the past few years allows to use AM in industry and not only in rapid prototyping as in the early days.

The big advantages compared to subtractive processes are design freedom, lightweight and stiffness tunable structures (lattices) and the possibility to easily customize or personalize parts without a significant increase in production costs.

Due to these reasons it is beneficial to use metal AM in the area of biomedical implants. Especially lattice structures with tunable properties have big potential to reduce the disadvantages of common implants. For example the risk of stress shielding can be removed by correct tuning of the lattice properties in the implant. Stress shielding is the effect of bone receding because of lack of load. An example of stress shielding can be seen in figure 1.1b. This could be prevented with an implant design similar to figure 1.1a.

In addition to the reduction of stress shielding, another big advantage of lattice structures in biomedical implants is the possibility of bone ingrowth. With the right porous geometry of the lattice structures, a significant ingrowth of bone can be observed already after a few weeks (Arabnejad et al. [2016]).

Next to all those advantages there is a big challenge: due to the manufacturing process induced defects, additively manufactured parts have an uncertainty in mechanical integrity. This uncertainty is especially critical in thin structures, where the size or diameter of the elements is at the lower limit of the technical feasibility dimensions in AM.

(a) AM hip implant with tunable lattice structure

(b) X-ray of a patient with signs of stress shielding (red circle) due to a conventional hip implant,
Burn [2016]

Figure 1.1: AM hip implant and stress shielding

1.2 Initial Situation and Objectives

The aim of this project was to create a good basis for further studies with available data and material from previous projects on this topic (Ghedalia [2019], Gillmann [2019], Greenfeld [2019] and Robmann [2019]).

To achieve this goal, two specific topics were covered: a constitutive model of additively manufactured Ti-6Al-4V with combined data of previous projects and mechanical testing of differently treated lattices.

Tensile and fatigue data of struts and lattices of the previous projects were used to determine in which direction this project would be heading. The available material for testing were horizontally printed lattices as seen in figure 1.2.

The lattices were manufactured with selective laser melting (SLM), the main

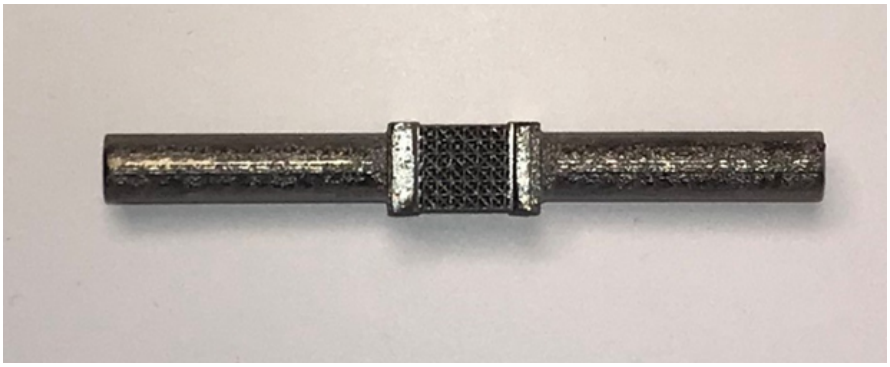

Figure 1.2: SLM manufactured horizontally printed lattice

loading axis oriented horizontally to the building direction. The properties of the basic raw material can be found in Appendix B.

Chapter 2

Materials and Methods

2.1 Constitutive Model for AM Ti-6Al-4V Lattices

2.1.1 Setup

19 struts from previous projects (Robmann [2019], Ghedalia [2019]) were used for underpinning the constitutive model. The meshed finite element geometries were already created from CT-data of the used struts and tensile tests were also executed. The surface mesh had an edge length of 0.05 mm. The used elements are both C3D4 (linear tetrahedron) and C3D10 (quadratic tetrahedron) depending on how many parameters were optimized. With only a few variable parameters quadratic elements were used and with a lot free parameters linear elements were used to moderate the computational cost. The struts were assembled in Abaqus as seen in figure 2.1. 16 struts were manufactured without geometry-mismatch compensation, with nominal diameters of 500 µm, 400 µm, 300 µm and 200 µm (y-direction, back to front) and printing orientations vertical, 60°, 30° and horizontal for each diameter (x-direction, left to right). The remaining 3 struts in the front row in figure 2.1 are also manufactured with a diameter of 200 µm, but with geometry-mismatch compensation. Printing orientations here were vertical, 45° and horizontal (first row, left to right).

Each strut was fixed at the bottom in all directions and fixed in x- and y-direction at the top, where an individual displacement in z-direction was applied for each strut at the top. The displacement was derived by measuring the total strain with help of digital image correlation (DIC) (figure 2.2) recorded during the tensile tests of the struts. The total displacement was derived from the measured strain and the height of the strut model.

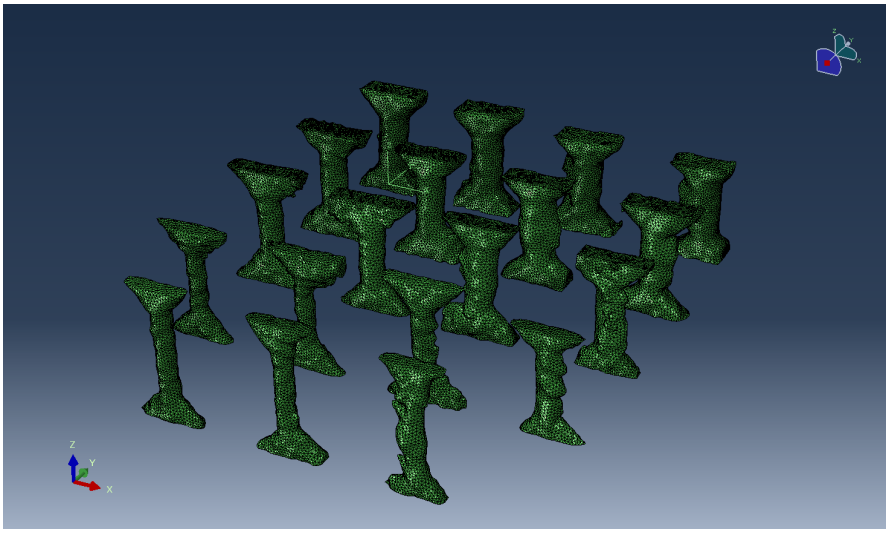

Figure 2.1: Setup for constitutive model calibration in Abaqus, in y-direction, back to front struts without geometry-mismatch compensation with diameter of 500 µm, 400 µm, 300 µm and 200 µm and in x-direction, left to right printing orientation vertical, 60°, 30° and horizontal for each diameter; first row, left to right struts with diameter 200 µm with geometry-mismatch compensation and printing orientations vertical, 45° and horizontal.

2.1.2 Experimental Data Preparation

To get a better starting position the experimental data of the tensile tests of the struts were resampled. The measured force and displacement points of the tensile tests of each strut were plotted and a fitted curve was generated (figure 2.3) with help of equation 2.1. On this curve 50 points were generated with the Matlab function *linspace* so that 19 datasets of the same format were available to work with.

2.1.3 Material Parameter Optimization

With the above-mentioned setup and resampled experimental data the material parameter optimization was started. The schematic diagram of the optimization can be seen in figure 2.4. In the beginning Matlab was fed with initial guesses for material parameters. Matlab ran with those parameters the Abaqus simulation. The simulation results were then compared to the experimental ones and a total error was calculated. Matlab then tried to minimize this error by adapting the material parameters with its function *fminsearch*.

In the beginning the model was kept isotropic but with time it needed to

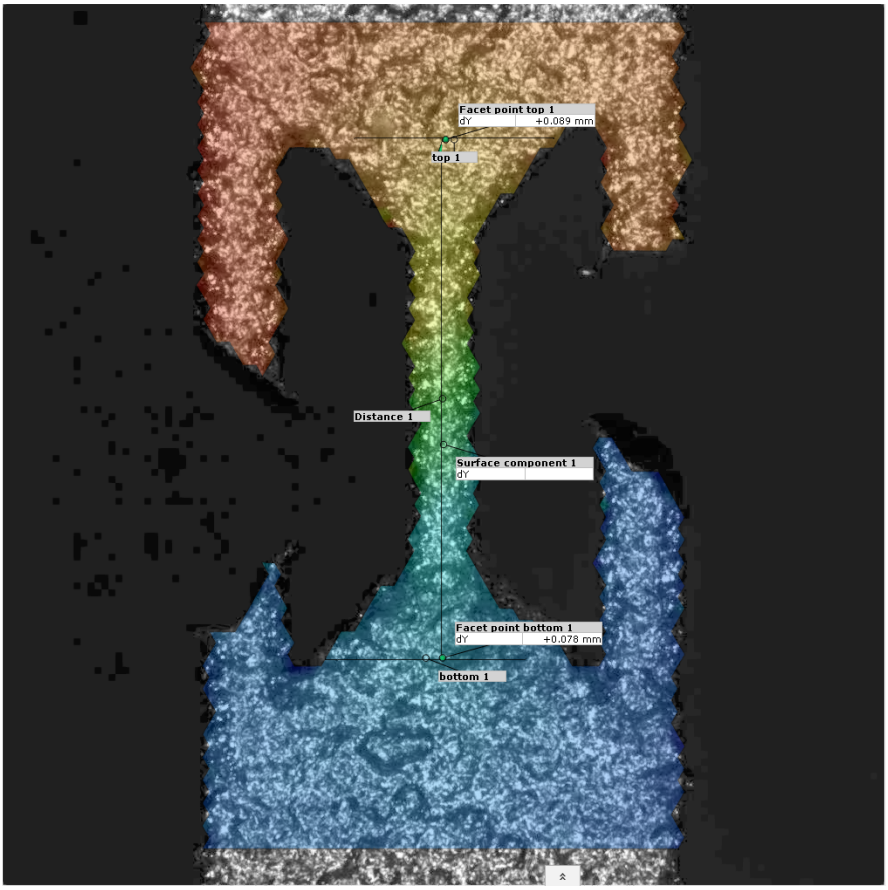

Figure 2.2: DIC displacement measurement of struts

$$\varepsilon_t = \frac{\sigma}{E} + A(\sigma - \sigma_0)^n \tag{2.1}$$

Total strain equation used for curve fitting in data resampling

be changed to transversely isotropic. A transversely isotropic model makes sense for AM material due to the anisotropy induced from the manufacturing process. The material properties are different in building direction than in its orthogonal direction.

In Abaqus engineering constants were used for the elasticity, the plasticity was modeled via tabular data (Armstrong-Frederick model) and anisotropic yielding with the Hill's potential function.

As the results were not satisfying, later during the optimization a size dependency had to be implemented by using field variables in the model.

To control the results of the optimization, the calculated parameters were

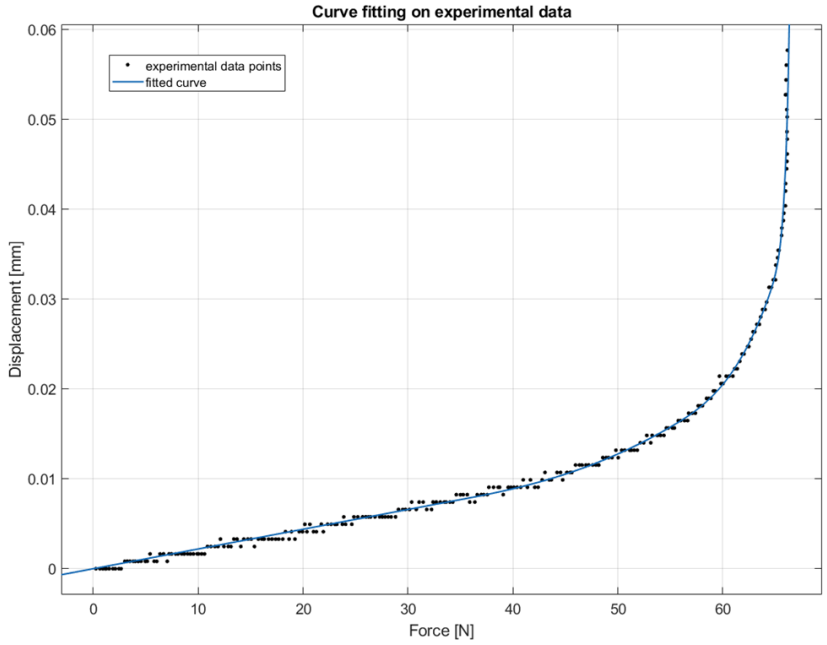

Figure 2.3: Curve fitting with adapted total strain equation (2.1) for data resampling

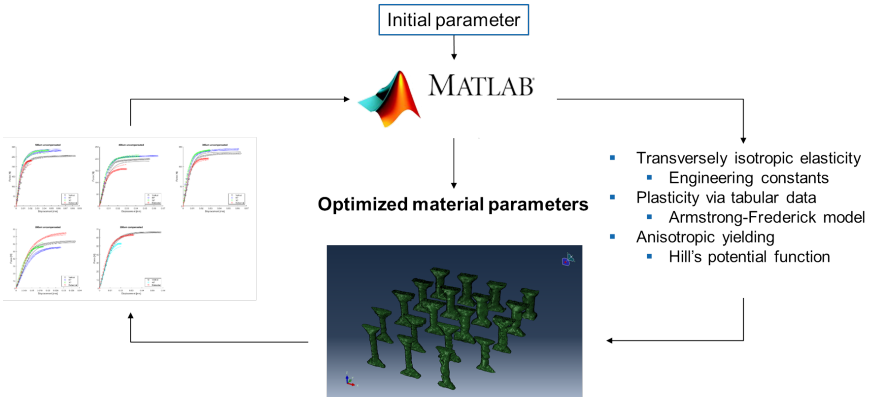

Figure 2.4: Schematic overview of the optimization

$$\begin{Bmatrix} \varepsilon_{11} \\ \varepsilon_{22} \\ \varepsilon_{33} \\ \gamma_{12} \\ \gamma_{13} \\ \gamma_{23} \end{Bmatrix} = \begin{bmatrix} 1/E_p & -\nu_p/E_p & -\nu_{tp}/E_t & 0 & 0 & 0 \\ -\nu_p/E_p & 1/E_p & -\nu_{tp}/E_t & 0 & 0 & 0 \\ -\nu_{tp}/E_p & -\nu_{tp}/E_p & 1/E_t & 0 & 0 & 0 \\ 0 & 0 & 0 & 1/G_p & 0 & 0 \\ 0 & 0 & 0 & 0 & 1/G_t & 0 \\ 0 & 0 & 0 & 0 & 0 & 1/G_t \end{bmatrix} \begin{Bmatrix} \sigma_{11} \\ \sigma_{22} \\ \sigma_{33} \\ \sigma_{12} \\ \sigma_{13} \\ \sigma_{23} \end{Bmatrix}$$

Transverse isotropy as defined in the ABAQUS *documentation*

$$f(\sigma) = \sqrt{F(\sigma_{22}-\sigma_{33})^2 + G(\sigma_{33}-\sigma_{11})^2 + H(\sigma_{11}-\sigma_{22})^2 + 2L\sigma_{23}^2 + 2M\sigma_{31}^2 + 2N\sigma_{12}^2}$$

Hill's potential function as defined in the ABAQUS *documentation*

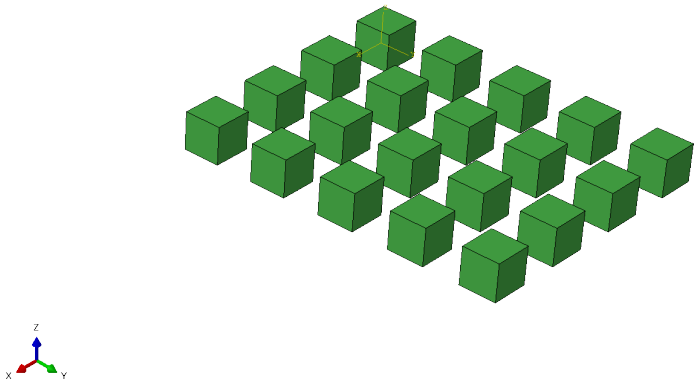

Figure 2.5: Cube assembly to verify material parameters, in x-direction from back to front the different sizes (500 µm, 400 µm, 300 µm and 200 µm) and in y-direction the different material orientations from left to right (vertical, 60°, 45°, 30° and horizontal)

implemented in 1 mm × 1 mm cubes (element type C3D8R) (fig. 2.5) with the specific size dependent material parameters and material orientation. The cubes were fixed at the bottom in all directions and at the top in x- and y-direction. Further a displacement of 0.1 mm was applied to the top. With MATLAB the stress - strain curves were plotted and possible errors could be evaluated. This setup was chosen to see the application of the different material parameters applied to the same model.

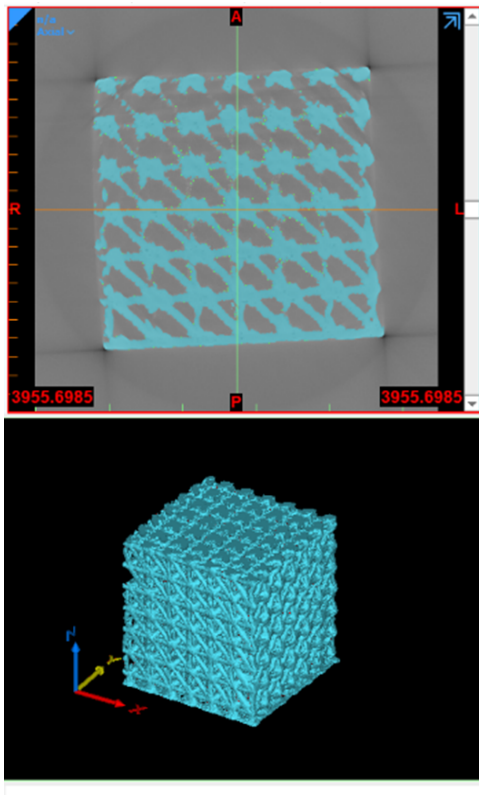

Figure 2.6: Screenshot of the Mimics software used to create 3D models from CT-scans.

2.2 Lattice Model

To create FE-models of the lattices, a CT-scan of the actual used lattices was performed. For each lattice a set of around 1200 images was created. These images were then imported to the the software Mimics (Materialise, Leuven, Belgium). Mimics works with different greyscale values. By setting the lower and upper limit of the greyscale the software can differentiate wheter a pixel is solid (material) or not. With this information different masks are created. With those masks defined for each image the software is creating a 3D model (figure 2.6).

After the model was created, it was imported to the software 3matic (Materialise, Leuven, Belgium). As only the lattice part of the specimen was scanned, the first step was to add the connectors to the part. With the full part ready the model could be meshed. The specific steps are described in Robmann [2019] chapter 3.1.4. As soon as those steps are done the model looks approximately like in figure 2.7 (cut view).

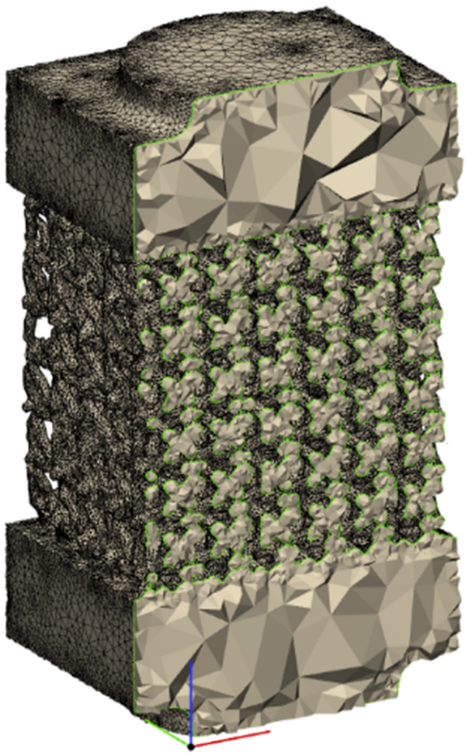

Figure 2.7: Cut view of a 3D meshed lattice model

2.3 Experiments

2.3.1 Test Setup

For all mechanical tests a walter+bai (Löhningen, Switzerland) testing machine (figure 2.8) was used. Equipped with a load cell (maximum force of 100 kN) for the load measurement and a 15 mm extensometer (Epsilon Technology Corp, Jackson, USA) for the strain measurement. For fatigue tests a R-ratio of 0.1 was used and for the tensile tests additionally to the standard setup an eo-2323 camera with a techspec gold series focusable telecentric lens (edmund optics, Barrington, New Jersey) for DIC measurements was used.

DIC was used to get the local and total displacements of the lattice. The local displacements were used to analyze the behaviour in the lattice and the maximum displacement was used for the simulation of the lattice model with the optimized material parameters.

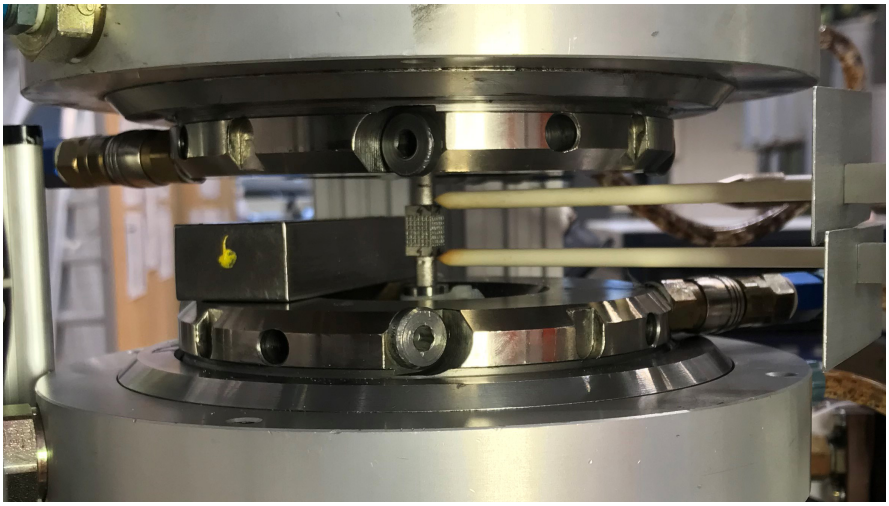

Figure 2.8: Test setup for fatigue and tensile tests with extensometer

2.3.2 Material

The available lattices for this project were differently treated after manufacturing so that three different groups were formed: raw, etched and epoxy filled (figure 2.9).

The raw lattices didn't get any special post processing after manufacturing.

The etched ones were previously chemically etched in Kroll's reagent, consisting of 100 ml distilled H_2O, 2 ml HNO_3 (65%) and 3 ml HF (40%) for 7:30 minutes. To determine the duration of the etching a series of tests was performed. Test sample lattices were etched for 2:30, 5, 7:30 and 10 minutes and examined under a scanning electron microscope (SEM). The results can be seen in figure 2.10. The longer the etching duration, the smoother the struts of the lattices, but also the thinner they become. As the main goal was to smooth the surface and in the 5-minute-images there are still rough spots and by 10 minutes the struts are already very thin the decision fell on 7:30 minutes. The idea behind the etching is, besides gaining a smoother surface, the fact that medically used implants are generally etched before use as well.

As seen in chapter 1.1 a big advantage of AM lattice structures is bone ingrowth. To get a first idea how the mechanical behaviour could change when filled with material, lattice samples were filled with epoxy. Before filling with epoxy, the lattices were also etched with Kroll's reagent for 7:30 minutes. The epoxy should simulate the ingrown bone which means in the optimal case it should have similar mechanical properties to *novo bone*. Like mentioned in Hedayati et al. [2017a] *novo bone* has a Young's modulus between 0.7 GPa and 1.5 GPa. The lattices were filled with 3M™ Scotch-Weld™ Structural Epoxy Adhesive EC-9323 B/A. The Young's modulus of

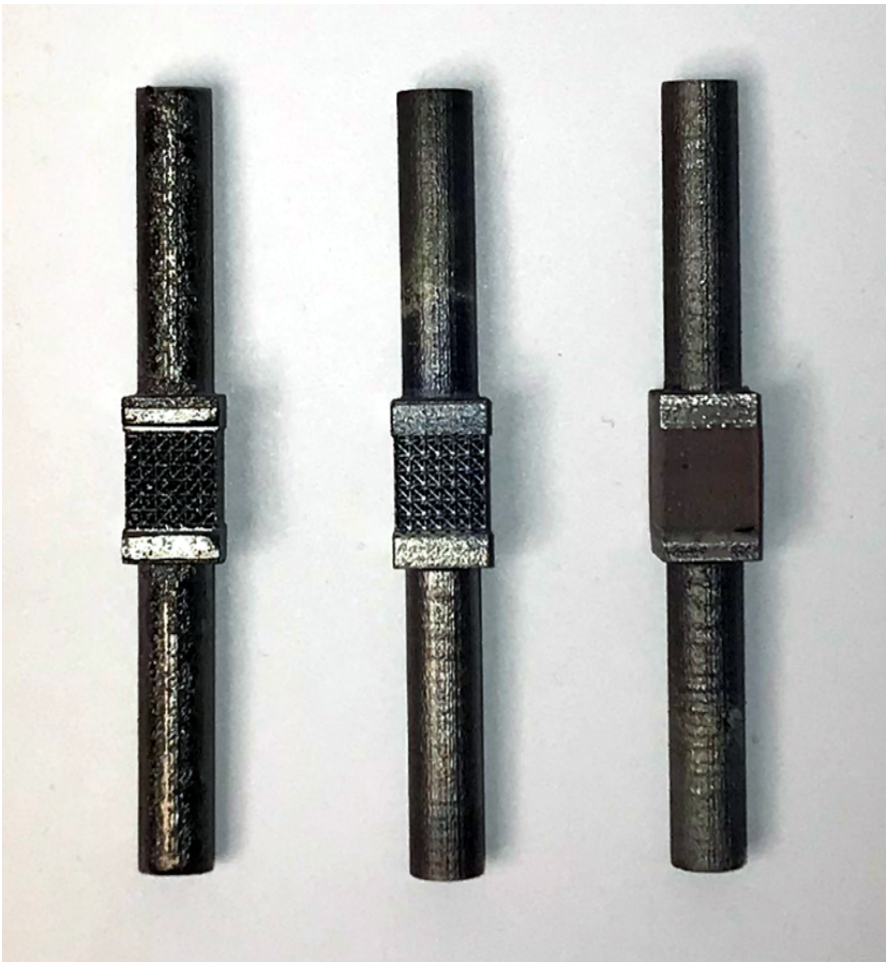

Figure 2.9: Overview of different lattices: raw, etched and epoxy filled (from left to right)

the epoxy was assumed to be around 2 GPa - 3 GPa (see Ermanni [2017]).

2.3.3 Simulation

For the simulation of the lattices the 3D models generated from CT scans were used. The material parameters were taken from the latest optimization. As the optimization was working with size dependency, the parameters of the 200 um struts were used. At the bottom fixed in all directions and at the top in x- and y-direction, the displacement measured with DIC was applied to the model and the FEA was run in Abaqus.

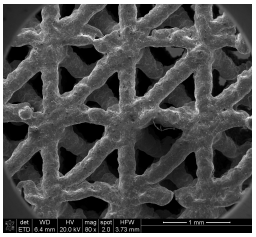

(a) Non etched, 80x magnification

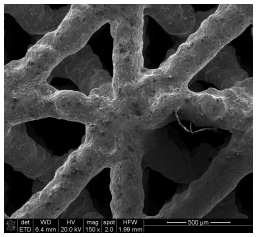

(b) Non etched, 150x magnification

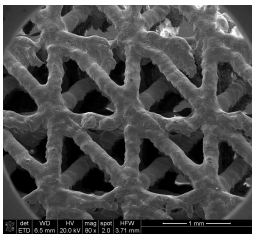

(c) 2:30 minutes, 80x magnification

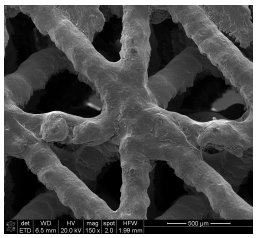

(d) 2:30 minutes, 150x magnification

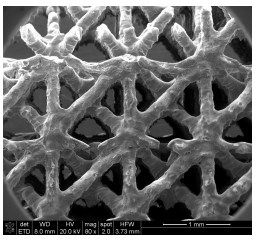

(e) 5 minutes, 80x magnification

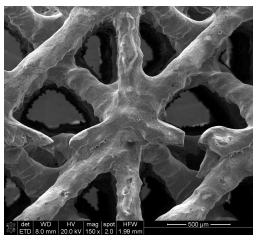

(f) 5 minutes, 150x magnification

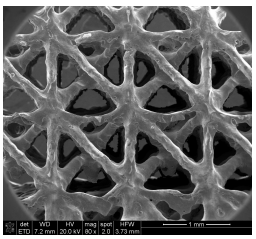

(g) 7:30 minutes, 80x magnification

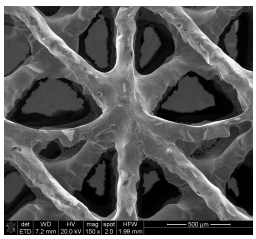

(h) 7:30 minutes, 150x magnification

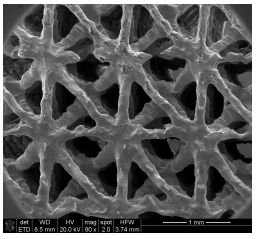

(i) 10 minutes, 80x magnification

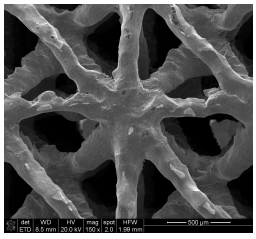

(j) 10 minutes, 150x magnification

Figure 2.10: Effect of different etching times on the surface of the lattice

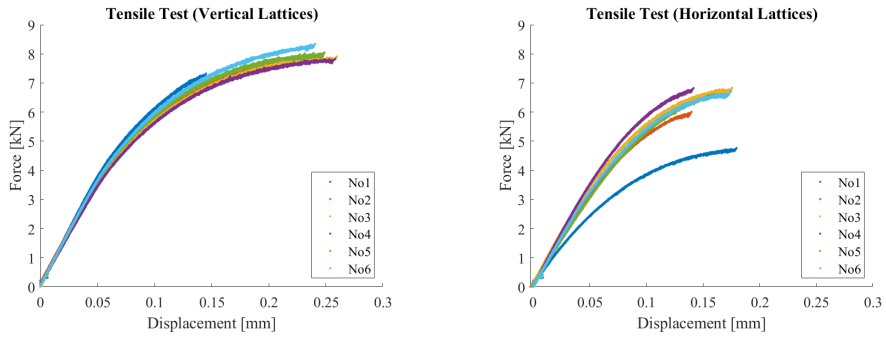

(a) Vertical lattices (b) Horizontal lattices

Figure 2.11: Tensile results of vertical and horizontal lattices (Robmann [2019])

2.3.4 Expectations

For the mechanical tests, tensile and fatigue, different behaviour was expected for each lattice type. Already known is the tensile behaviour of raw horizontal lattices compared to vertical lattices (figure 2.11, Robmann [2019]). As can be seen, the strength of horizontally manufactured lattices is around 20% weaker than the vertical ones. A similar fatigue behaviour of the horizontal compared to the vertical lattices is expected due to the fact that the average geometry won't differ too much from each other even though the printing directions are different.

Etching of the lattices results in a smoother surface which will have a positive impact on fatigue behaviour due to reduction of notch effects. But as the etching causes around 25% thinner struts the lattice structure is also weaker. Both effects considered the etched lattices are expected to have a similar fatigue life as raw lattices even if the strength will be lower.

For the epoxy filled lattices there were only few data in literature. Hedayati et al. [2017a] found that the fatigue life of filled lattice structures can be improved by factor 2 to 7 compared to empty lattices. To predict the elastic behaviour of epoxy filled lattices the formula for composite materials was used (formula 2.2).

$$E_{tot} = E_{Ti-6Al-4V} \times v_{Ti-6Al-4V} + E_{Epoxy} \times v_{Epoxy} \tag{2.2}$$

With a measured porosity of around 65% (Robmann [2019]), an assumed Young's modulus of the epoxy $E_{Epoxy} = 3\,\text{GPa}$ and a Young's modulus $E_{Ti-6Al-4V} = 120\,\text{GPa}$ for the metallic part results with equation 2.2

$$E_{theoreticalraw} = 42\,\text{GPa}$$

for the raw lattice and

$$E_{theoreticalepoxy} = 44\,\text{GPa}$$

for the epoxy filled lattices. With this approach an increase of 5%-10% in stiffness could be predicted. For the fatigue behaviour this increase in strength is not decisive but the notch effects decrease because of the epoxy which will result in higher fatigue life.

Chapter 3

Results

3.1 Constitutive Model for AM Ti-6Al-4V Lattices

3.1.1 Material Optimization

The results of the material model parameter optimization can be seen in figure 3.1. The lines are the simulation results with the optimized material parameters and the circles are the actual (resampled) test results. What catches the eye is that the 500 µm, 400 µm and 300 µm test results have a similar order. Meaning the horizontal strut is the weakest and the vertical and 60° struts the strongest. This order changes dramatically regarding the 200 µm struts, both in the geometry mismatch compensated and uncompensated samples. This random order is because 200 µm structures are the lower manufacturing limit when using SLM. Due to this fact a big scatter occurs in geometry and so the strength of the struts with 200 µm diameter varies between every sample.

It appears that the elastic part of the results is matching quite well unlike the plastic part where there is still a considerable error.

Looking at the results of the stress strain curves of the cube assembly (see section 2.1.3) in figure 3.2 a similar behaviour as in the displacement force curves of the struts can be observed. 500 µm, 400 µm and 300 µm have a similar order and in the 200 µm cubes the results seems randomly distributed.

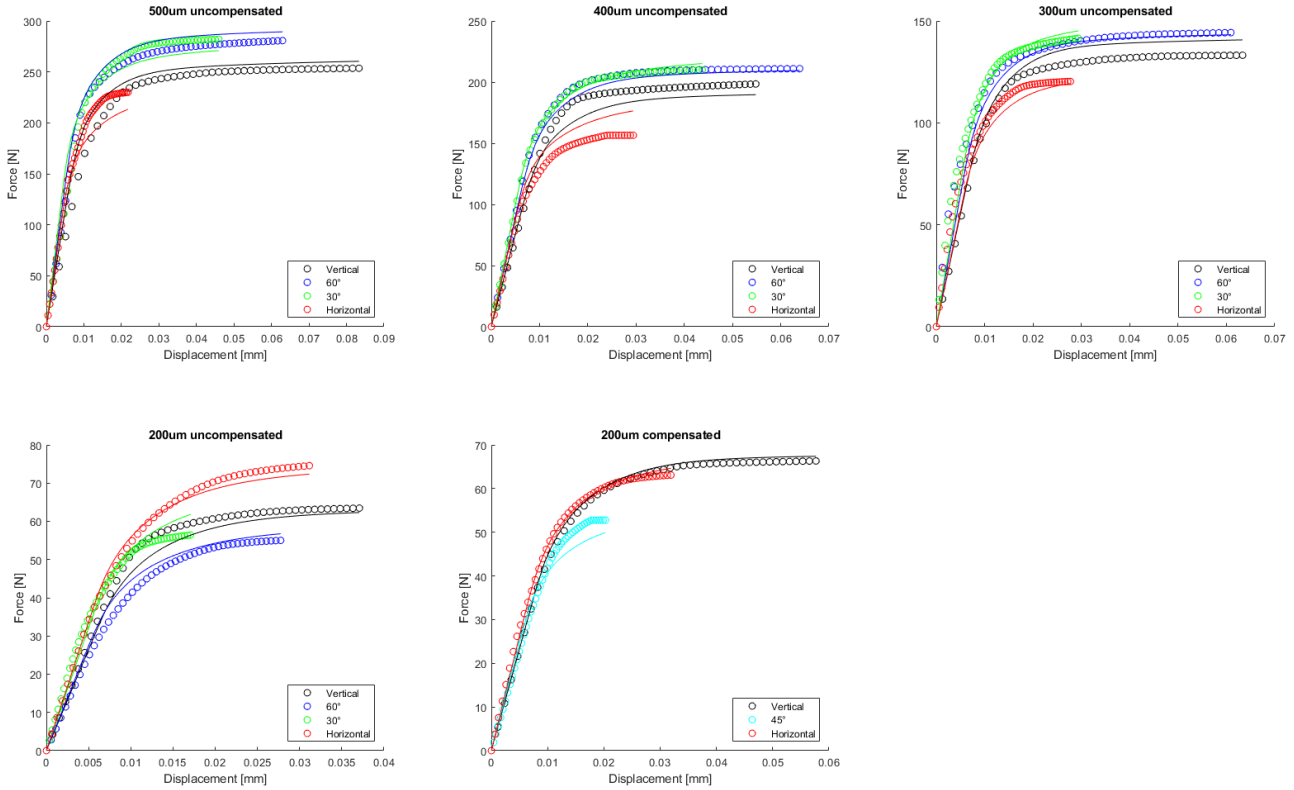

Figure 3.1: Displacement-force curves of resampled test results (o) and simulation with optimized parameters (-) of struts used for the constitutive model

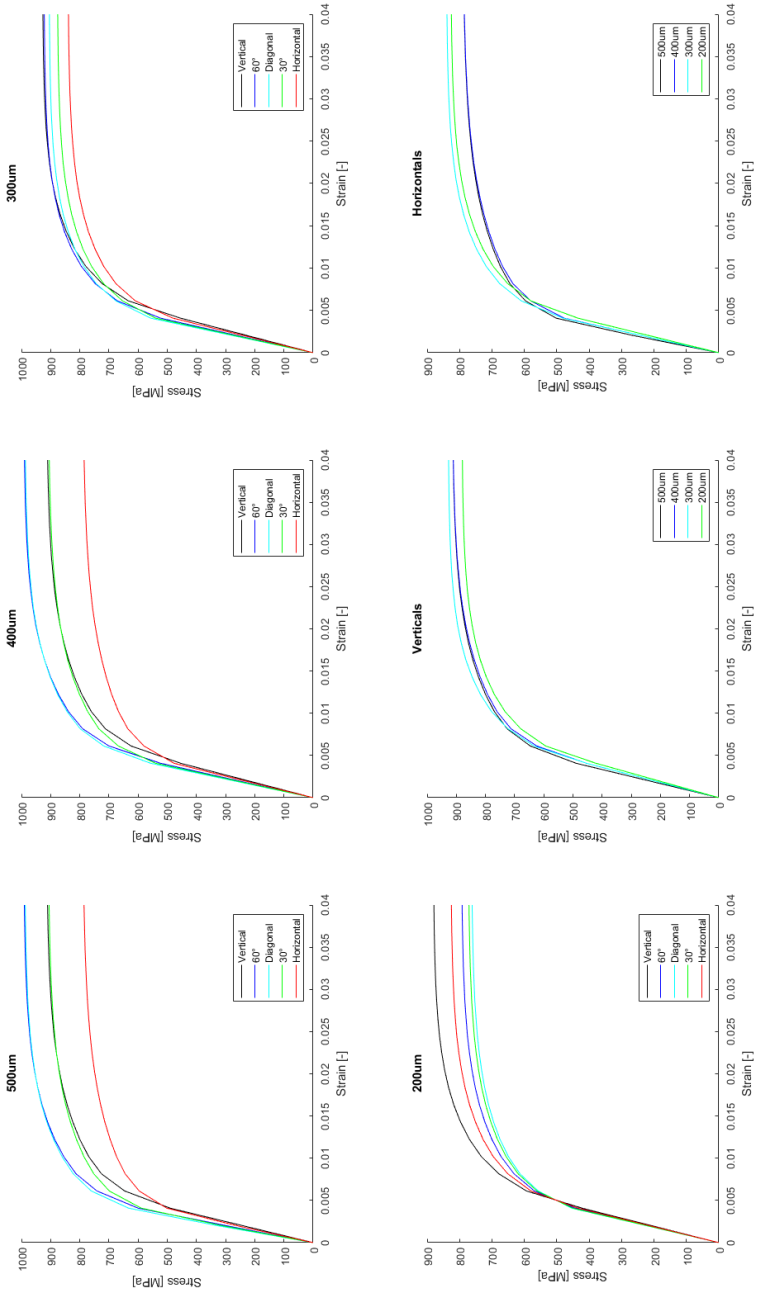

Figure 3.2: Stress-strain curves of the cube assembly to verify the results of the optimization

3.2 Experimental Results

3.2.1 Tensile tests

In figure 3.3 the graphic results of DIC tracking and the simulation of the same lattice can be seen. As visible in both DIC and simulation the maximum strain is in the struts parallel to the load direction (figure 3.3).

Lattice type	**F_{max} [N]**	**Displacement at F_{max} [mm]**
raw	7276	0.1999
etched	6609	0.2000
epoxy filled	9957	0.2133

Table 3.1: Tensile results of lattices

The tensile and simulation results for each lattice types are shown in figures 3.4, 3.5 and 3.6 and table 3.1. The maximum force of the etched lattice is around 10% lower in comparison to the raw lattice even with 25% thinner struts. The strength of the epoxy filled sample is around 30% higher than the raw lattice also when the expected increase in stiffness was only 5%-10%. Interestingly all types of lattices start failing at nearly the same displacement of around 0.2 mm. When calculating the Young's modulus of the lattices (area $A_{lattice} = 7.4\,\text{mm} \times 7.4\,\text{mm} = 54.76\,\text{mm}^2$) with these test results at the force $F = 2000\,\text{N}$ following values will result:

$$E_{raw} = 10.7\,\text{GPa} \qquad E_{etched} = 9.3\,\text{GPa} \qquad E_{epoxy} = 14.6\,\text{GPa}$$

For simulations calculated parameters were used from the optimization (section 3.1.1) and also the lattice model is the same as the actual tested sample, meaning it is generated from the CT scan of the actual lattice. It can clearly be seen that the simulation results correspond with the mechanical test results at maximum force. The elastic part of the curve is overestimated. For the epoxy filled lattice a simulation failed already during creation of the 3D model. Creating the 3D model of both lattice and epoxy worked in Mimics using the non-manifold-assembly tool. Problems occured using 3matic as the software was not able to handle the big data of the generated model. With the available software it was not possible to mesh the model for epoxy filled lattices.

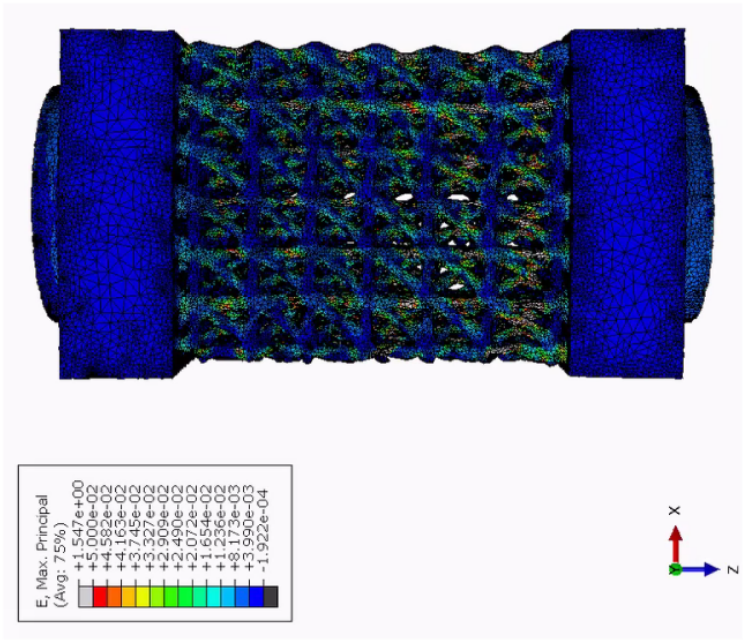

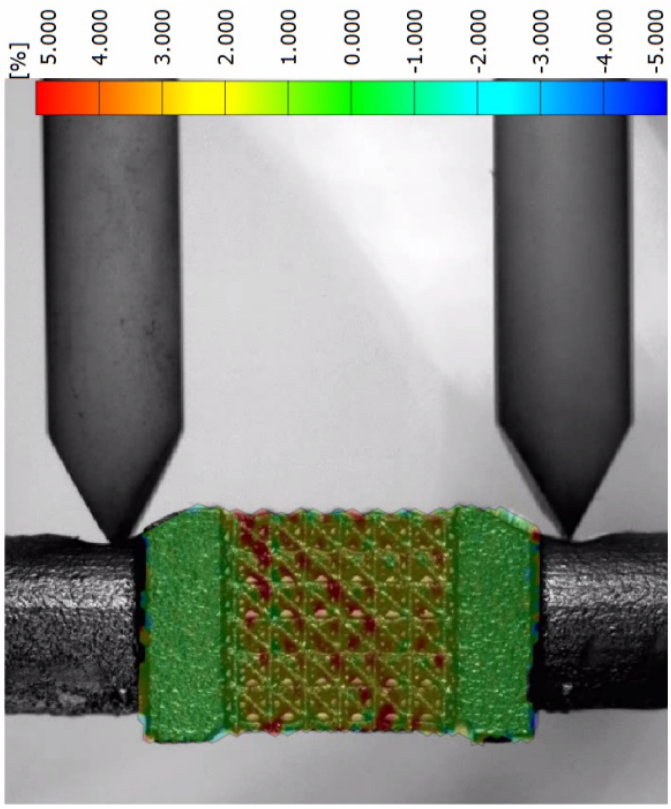

Figure 3.3: Comparison of real strain using DIC measurements during tensile testing (left) and ABAQUS simulation (right) of the identical lattice

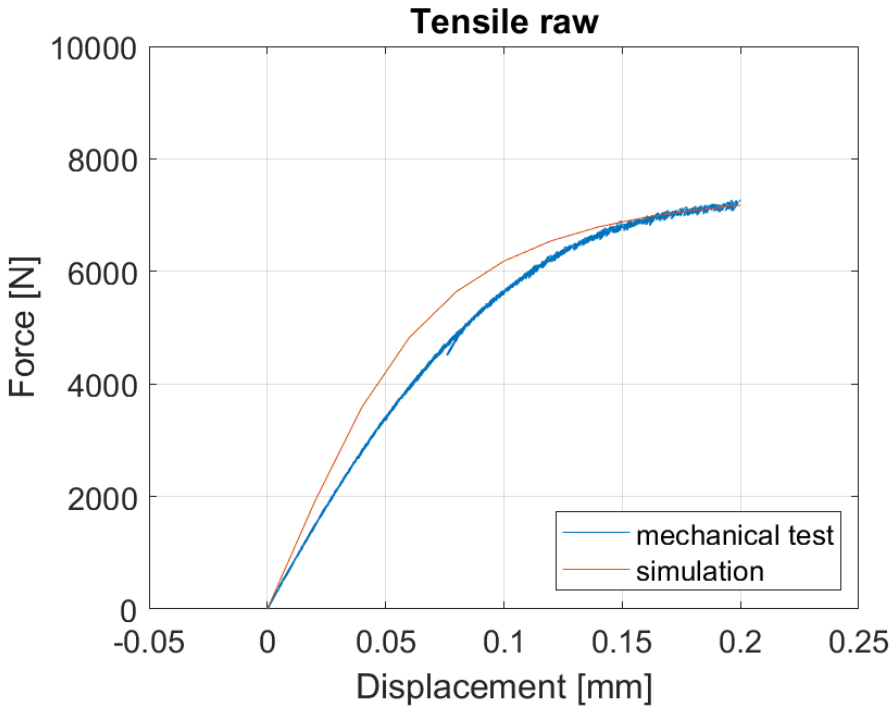

Figure 3.4: Tensile test and simulation results for a raw lattice

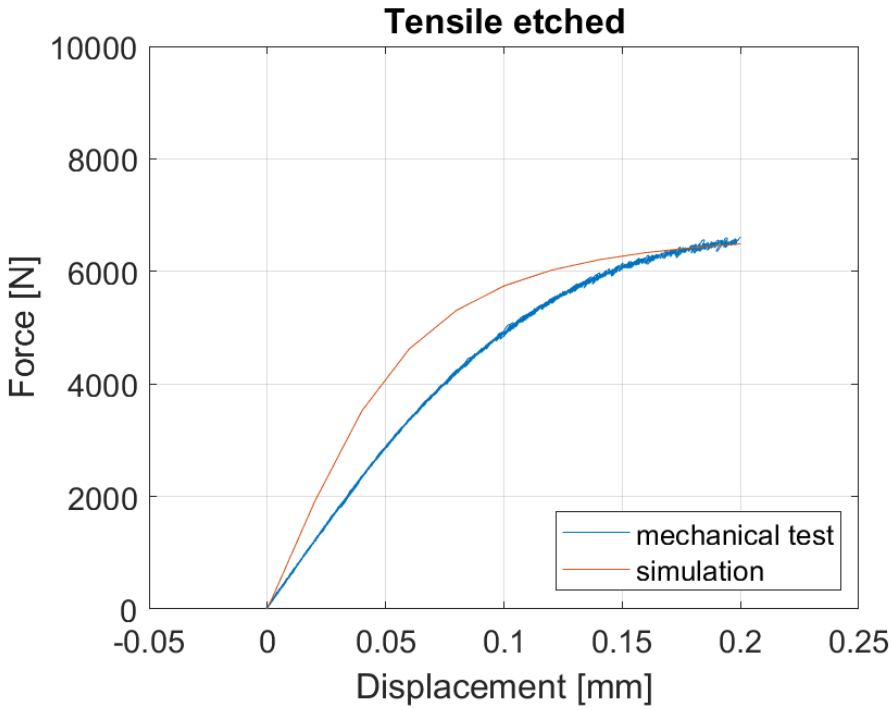

Figure 3.5: Tensile test and simulation results for an etched lattice

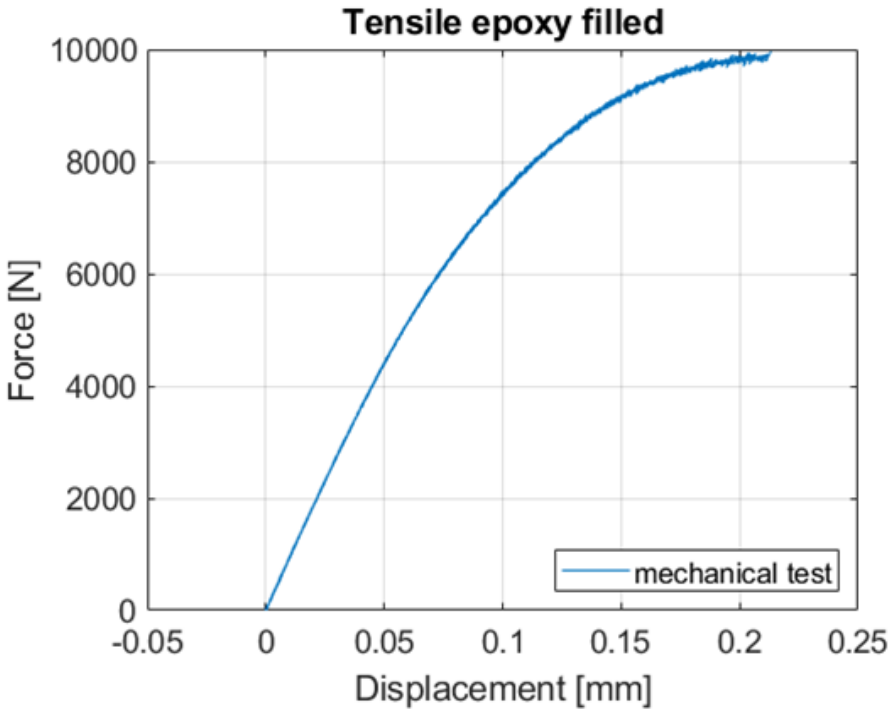

Figure 3.6: Tensile test results for an epoxy filled lattice

3.2.2 Fatigue tests

The fatigue behaviour of the different lattices is shown in figure 3.7 using force amplitude. The data of the vertical lattices are taken from Greenfeld [2019]. As expected the vertical and horizontal lattices have a similar fatigue behaviour. The etched samples are a bit lower but still in a similar range. What was surprising is that epoxy filled lattices have $10-20\times$ longer fatigue life than raw samples. Also when the strength is only 30% higher.

To get a better understanding of these results they are plotted in figure 3.8 using fatigue ratio instead of force amplitude (force amplitude divided by maximum force of the tensile test). Vertical, horizontal (raw) and etched samples are now very close to each other while the epoxy filled lattices still have an around $10\times$ longer fatigue life.
What can be determined clearly is that all lattice results have a significant lower fatigue life than wrought and bulk AM Ti-6Al-4V.

Lattice type	Force Amplitude [N]	Fatigue Ratio	Cycles [-]	
raw	350	0.048105078	1000000	run out
raw	375	0.051541155	782154	
raw	400	0.054977232	358576	
raw	600	0.082465848	68515	
raw	900	0.123698772	22083	
etched	300	0.045391767	5000000	run out
etched	350	0.052957062	625609	
etched	400	0.060522356	343385	
etched	800	0.121044713	4802	
epoxy filled	600	0.060257551	2000000	run out
epoxy filled	800	0.080343402	2000000	run out
epoxy filled	900	0.090386327	844897	
epoxy filled	1000	0.100429252	127009	
epoxy filled	1200	0.120515103	118211	

Table 3.2: Fatigue results of lattices

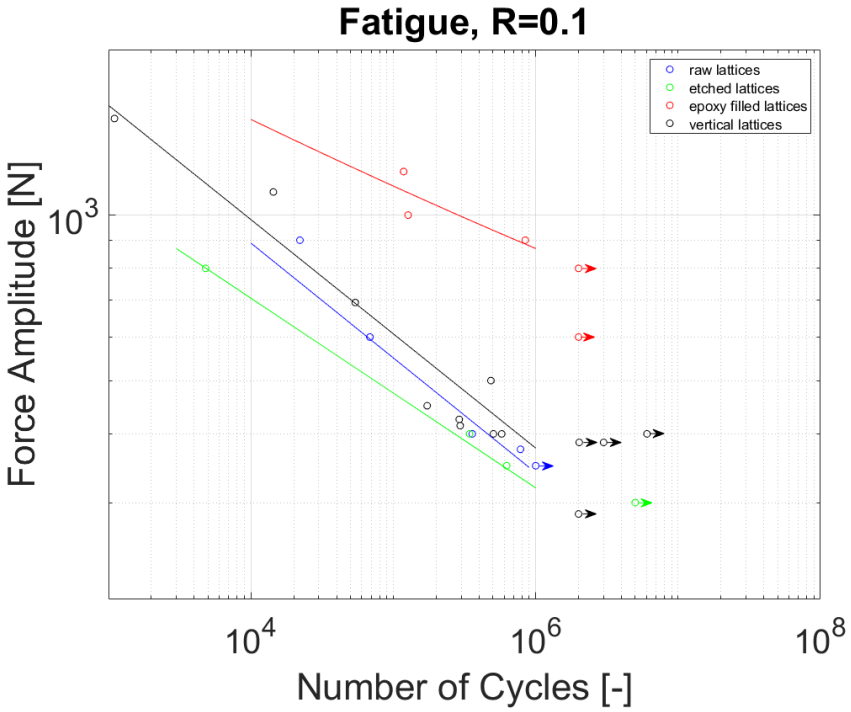

Figure 3.7: Fatigue results of different lattices plotted with force amplitude

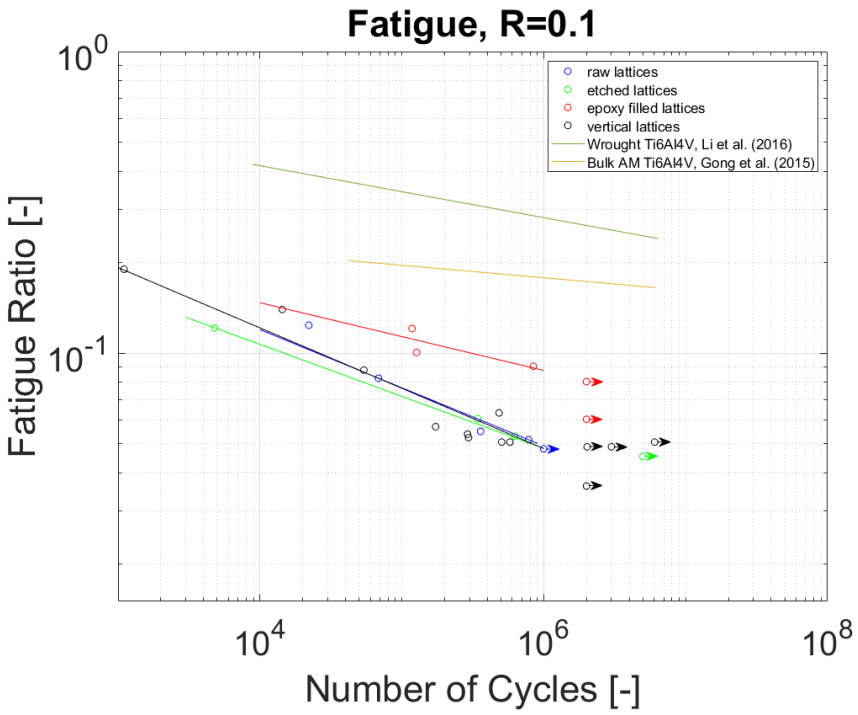

Figure 3.8: Fatigue results of different lattices plotted with fatigue ratio

Chapter 4

Discussion

4.1 Constitutive Model for AM Ti-6Al-4V Lattices

The performance of the constitutive model applied on the lattices was quite good considering the maximum force and displacement. But the elastic part of the curve was steeper in the simulation, which means the Young's modulus is overestimated in the model.

Geometries manufactured at the lower limit of SLM (200 µm) have usually a big error compared to the nominal model. In the case of printing thin struts the error is even bigger when the geometries are oriented horizontally to the building direction. This results in over- and undersizing of the struts. Meaning there are parts in the struts which are way too thick and others which are too thin or even have a gap. Those geometrical errors lead to notch effects or open struts which can initiate a crack in the whole lattice. Regarding the material parameter optimization this effect has a big disadvantage. In the setup used in this project seven (200 µm) struts were used, from which only two were horizontally printed. Considering that the geometry of horizontally printed struts is in most cases random it is difficult to optimize parameters considering only two specimens. The same applies to 30°, 45°, 60° and vertical struts but the most extreme are the horizontal ones. The implementation of size dependency originates in the above mentioned effect. Maybe with more 200 µm struts in the setup a general trend could be observed and with an optimization running on these a better prediction on the behaviour of the lattices could be made.

4.2 Experiments

4.2.1 Tensile tests

The result of the horizontal raw tensile test is a bit higher than expected. Due to the topic discussed above and the fact that in the lattices the most loaded struts are the ones in direction of loading, there must be a bigger scatter in the results of the horizontally manufactured lattices. The mainly loaded struts have significant geometrical errors and therefore a scatter in the results. This seems to be the main reason for the test result of the horizontal lattice tested in this project compared to the ones tested in Robmann [2019].

Regarding the etched samples this effect is even more significant. As the etching causes 25% thinner struts it is well possible that some parts can be dissolved completely during the etching. This is a relevant side effect of the main advantage of etching. By etching a surface powder particles and irregularities can be smoothed and minimize notch effects, which improve the mechanical properties of the lattice.

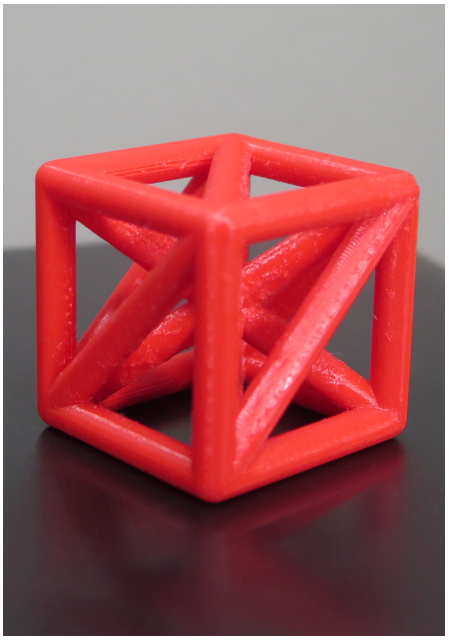

Figure 4.1: Unit cell model of the lattices manufactured with fused deposition modeling (FDM)

Another phenomenon could be observed in the epoxy filled lattices. The calculation predicts a $5\% - 10\%$ higher stiffness than a raw lattice. But the measured stiffness shows a completely different picture. The stiffness of the epoxy filled lattices is around 30% higher than of the raw lattices. This effect could be explained by the fact that either the epoxy is way stronger than assumed or the epoxy prevents the lattice structure from compression and tension and thus strengthens the stiffness.

For all lattice types the calculated Young's modulus (chapter 2.3.4) are $3 - 4\times$ higher than the measured ones (chapter 3.2.1). To explain this phenomenon a look at the unit cell from which the lattices are built is necessary. A unit cell of the lattices (figure 4.1) consists of 22 struts. Only 4 of the struts are in vertical direction, 8 in diagonal and 10 horizontal to the load case used in this project. As already mentioned before most of the load is taken by the struts in load direction (vertical). A small part by the diagonal ones and

barely any load is taken by the horizontal struts. This information could possibly explain why the measured Young's modulus is only 25%-30% of the calculated one.

4.2.2 Fatigue tests

The fatigue results for the raw and the etched lattices fitted roughly in the expectations made before the tests. The according curves are already found very close when plotting with force amplitude and nearly overlapping when regarding the fatigue ratio. So it seems that with etching the notch effects are clearly reduced. Even with 25% thinner struts a similar fatigue behavior is achieved as with raw lattices. A bit different is the situation with the epoxy filled lattices. With a 30% higher stiffness a $10 - 20\times$ higher fatigue life is reached. This result can not only originate in the higher stiffness. It is more probable that the notch effects disappeared nearly completely through filling the gaps with epoxy. Another explanation could be the stiffening through preventing the lattice from compression and tension as mentioned before. Because of the higher Young's modulus the strain in the lattice is also lower, which has also a positive influence on fatigue life.

Chapter 5

Outlook

5.1 Simulation

Regarding development of the constitutive model for AM Ti-6Al-4V the setup could be changed in a way that more samples of every strut type are included in the simulation and not just one as it is done in the present setting. With several thin (200 µm) struts for each building direction the scatter could be taken into account and hopefully lead to a better result in the end.

Another approach to develop a constitutive model would be to simulate unit cells or lattice parts and optimize them. The difficulty here would be to get to the exact test results of the chosen cell(s). As we only know the total reaction forces of tested lattices it would be difficult to derive the reaction forces of one unit cell. To simulate the whole lattice would be another solution but it would be computationally very expensive. Maybe a solution would be to simulate several unit cells using a calculated mean force.

For the simulation of the epoxy filled lattices it was not possible with the current solution to mesh the model and work with it. Here either another approach needs to be found or the created model needs to be adapted so that 3matic can handle it, meaning the data size of the model should be somehow reduced or another setup or another software should be chosen to solve this problem. For the simulation more precise material data of the epoxy is required. The data can be determined by mechanical tests of epoxy samples. Another problem was the DIC tracking of the epoxy filled lattices. The surface of the epoxy was too even to allow DIC tracking. Even with manually added points the problem was not solved. In addition to that the epoxy started to whiten as the epoxy starts to fail. A possible solution would be to work with a transparent epoxy where small intransparent beads could be added to create a structure. This would possibly allow to track the

sample until the whitening starts.

5.2 Experiments

In general more specimens of each lattice type need to be tested. The results in this project are a good basis but they need to be verified with more tests to be statistically significant.

Regarding the etching process of the lattices a disadvantage was the thinning of the struts so the results are difficult to compare to the raw samples. An idea would be to produce the lattices with thicker struts and in post processing etch them to nominal size. It would be interesting as well to analyze the difference of etched lattices both vertical and horizontal. With thin struts (200 µm) the effect on horizontal lattices is more serious than on vertical ones because of geometrical errors during manufacturing.

To find out why the epoxy filled lattices perform so much better in fatigue life than the others, a possibility would be to put a thin layer over the lattice and compare it with the fully filled samples. If the suppressed notch effect is responsible for this bahaviour, the thin layer should have a similar behaviour. If not the main reason might be the blocking of the movement of the lattice. The first case would be interesting for further studies as the fatigue life easily could be improved with a thin layer. Hypothethically an AM implant with lattice structures could be covered with a thin layer of biocompatible material to extend the fatigue life and still be accepted by the body.

List of Figures

1.1 AM hip implant and stress shielding 2
1.2 SLM manufactured horizontally printed lattice 3

2.1 Setup for constitutive model calibration in ABAQUS, in y-direction, back to front struts without geometry-mismatch compensation with diameter of 500 µm, 400 µm, 300 µm and 200 µm and in x-direction, left to right printing orientation vertical, 60°, 30° and horizontal for each diameter; first row, left to right struts with diameter 200 µm with geometry-mismatch compensation and printing orientations vertical, 45° and horizontal. 6
2.2 DIC displacement measurement of struts 7
2.3 Curve fitting with adapted total strain equation (2.1) for data resampling 8
2.4 Schematic overview of the optimization 8
2.5 Cube assembly to verify material parameters, in x-direction from back to front the different sizes (500 µm, 400 µm, 300 µm and 200 µm) and in y-direction the different material orientations from left to right (vertical, 60°, 45°, 30° and horizontal) 9
2.6 Screenshot of the Mimics software used to create 3D models from CT-scans. 10
2.7 Cut view of a 3D meshed lattice model 11
2.8 Test setup for fatigue and tensile tests with extensometer 12
2.9 Overview of different lattices: raw, etched and epoxy filled (from left to right) 13
2.10 Effect of different etching times on the surface of the lattice . . . 14
2.11 Tensile results of vertical and horizontal lattices (Robmann [2019]) 15

3.1 Displacement-force curves of resampled test results (o) and simulation with optimized parameters (-) of struts used for the constitutive model 18

3.2 Stress-strain curves of the cube assembly to verify the results of the optimization 19
3.3 Comparison of real strain using DIC measurements during tensile testing (left) and Abaqus simulation (right) of the identical lattice 21
3.4 Tensile test and simulation results for a raw lattice 22
3.5 Tensile test and simulation results for an etched lattice 22
3.6 Tensile test results for an epoxy filled lattice 23
3.7 Fatigue results of different lattices plotted with force amplitude . 24
3.8 Fatigue results of different lattices plotted with fatigue ratio . . . 25

4.1 Unit cell model of the lattices manufactured with fused deposition modeling (FDM) 28

List of Tables

3.1 Tensile results of lattices 20
3.2 Fatigue results of lattices 24

Bibliography

S.M. Ahmadi, R. Hedayati, Y. Li, K. Lietaert, N. Tümer, A. Fatemi, C.D. Rans, B. Pouran, H. Weinans, and A.A. Zadpoor. Fatigue performance of additively manufactured meta-biomaterials: The effects of topology and material type. *Acta Biomaterialia*, 65:292 – 304, 2018. ISSN 1742-7061. doi: https://doi.org/10.1016/j.actbio.2017.11.014. URL http://www.sciencedirect.com/science/article/pii/S1742706117306980.

S.M. Ahmadi, R. Kumar, E.V. Borisov, R. Petrov, S. Leeflang, Y. Li, N. Tümer, R. Huizenga, C. Ayas, A.A. Zadpoor, and V.A. Popovich. From microstructural design to surface engineering: A tailored approach for improving fatigue life of additively manufactured meta-biomaterials. *Acta Biomaterialia*, 83:153 – 166, 2019. ISSN 1742-7061. doi: https://doi.org/10.1016/j.actbio.2018.10.043. URL http://www.sciencedirect.com/science/article/pii/S1742706118306421.

Sajad Arabnejad, R. Burnett Johnston, Jenny Ann Pura, Baljinder Singh, Michael Tanzer, and Damiano Pasini. High-strength porous biomaterials for bone replacement: A strategy to assess the interplay between cell morphology, mechanical properties, bone ingrowth and manufacturing constraints. *Acta Biomaterialia*, 30:345 – 356, 2016. ISSN 1742-7061. doi: https://doi.org/10.1016/j.actbio.2015.10.048. URL http://www.sciencedirect.com/science/article/pii/S174270611530177X.

P. James Burn. Current and future use of custom implants in orthopaedic surgery. The 12th Annual Orthopaedic Manufacturing Technology Exposition and Conference (OMTEC), Chicago, 2016.

Charlotte de Formanoir, Mathieu Suard, Rémy Dendievel, Guilhem Martin, and Stéphane Godet. Improving the mechanical efficiency of electron beam melted titanium lattice structures by chemical etching. *Additive Manufacturing*, 11:71 – 76, 2016. ISSN 2214-8604. doi: https://

doi.org/10.1016/j.addma.2016.05.001. URL http://www.sciencedirect.com/science/article/pii/S2214860416300847.

Joep de Krijger, Calvin Rans, Brecht Van Hooreweder, Karel Lietaert, Behdad Pouran, and Amir A. Zadpoor. Effects of applied stress ratio on the fatigue behavior of additively manufactured porous biomaterials under compressive loading. *Journal of the Mechanical Behavior of Biomedical Materials*, 70:7 – 16, 2017. ISSN 1751-6161. doi: https://doi.org/10.1016/j.jmbbm.2016.11.022. URL http://www.sciencedirect.com/science/article/pii/S1751616116304131. Mechanics of additively manufactured biomaterials and implants.

Paolo Ermanni. Manufacturing of polymer composites - lecture script. Table 2.3, 2017.

Daniele Ghedalia. Characterization and modeling of orientation and size dependent tensile behavior of am Ti6Al4V. Master project, ETH Zürich, Zurich, Switzerland, 2019.

Alexander Gillmann. Fatigue behavior investigation of additively manufactured Ti-6Al-4V. Research project, ETH Zürich, Zurich, Switzerland, 2019.

Daniel Greenfeld. Fatigue behavior investigation of additively manufactured Ti-6Al-4V lattices. Research internship, ETH Zürich, Zurich, Switzerland, 2019.

R. Hedayati, S. Janbaz, M. Sadighi, M. Mohammadi-Aghdam, and A.A. Zadpoor. How does tissue regeneration influence the mechanical behavior of additively manufactured porous biomaterials? *Journal of the Mechanical Behavior of Biomedical Materials*, 65:831 – 841, 2017a. ISSN 1751-6161. doi: https://doi.org/10.1016/j.jmbbm.2016.10.003. URL http://www.sciencedirect.com/science/article/pii/S1751616116303526.

R. Hedayati, S. Amin Yavari, and A.A. Zadpoor. Fatigue crack propagation in additively manufactured porous biomaterials. *Materials Science and Engineering: C*, 76:457 – 463, 2017b. ISSN 0928-4931. doi: https://doi.org/10.1016/j.msec.2017.03.091. URL http://www.sciencedirect.com/science/article/pii/S0928493116315776.

R. Hedayati, H. Hosseini-Toudeshky, M. Sadighi, M. Mohammadi-Aghdam, and A.A. Zadpoor. Multiscale modeling of fatigue crack propagation in additively manufactured porous biomaterials. *International Journal of Fatigue*, 113:416 – 427, 2018. ISSN 0142-1123. doi: https://doi.org/10.1016/j.ijfatigue.2018.05.006. URL http://www.sciencedirect.com/science/article/pii/S0142112318301774.

Brecht Van Hooreweder and Jean-Pierre Kruth. Advanced fatigue analysis of metal lattice structures produced by selective laser melting. *CIRP Annals*, 66(1):221 – 224, 2017. ISSN 0007-8506. doi: https://doi.org/10.1016/j.cirp.2017.04.130. URL http://www.sciencedirect.com/science/article/pii/S0007850617301300.

Brecht Van Hooreweder, Yanni Apers, Karel Lietaert, and Jean-Pierre Kruth. Improving the fatigue performance of porous metallic biomaterials produced by selective laser melting. *Acta Biomaterialia*, 47:193 – 202, 2017a. ISSN 1742-7061. doi: https://doi.org/10.1016/j.actbio.2016.10.005. URL http://www.sciencedirect.com/science/article/pii/S1742706116305232.

Brecht Van Hooreweder, Karel Lietaert, Bram Neirinck, Nicholas Lippiatt, and Martine Wevers. CoCr F75 scaffolds produced by additive manufacturing: Influence of chemical etching on powder removal and mechanical performance. *Journal of the Mechanical Behavior of Biomedical Materials*, 68:216 – 223, 2017b. ISSN 1751-6161. doi: https://doi.org/10.1016/j.jmbbm.2017.02.005. URL http://www.sciencedirect.com/science/article/pii/S1751616117300620.

Serjosha Robmann. Deformation analysis and finite element modelling for Ti-6Al-4V additive manufactured lattices. Master's thesis, ETH Zürich, Zurich, Switzerland, 2019.

S. Amin Yavari, R. Wauthle, J. van der Stok, A.C. Riemslag, M. Janssen, M. Mulier, J.P. Kruth, J. Schrooten, H. Weinans, and A.A. Zadpoor. Fatigue behavior of porous biomaterials manufactured using selective laser melting. *Materials Science and Engineering: C*, 33(8):4849 – 4858, 2013. ISSN 0928-4931. doi: https://doi.org/10.1016/j.msec.2013.08.006. URL http://www.sciencedirect.com/science/article/pii/S0928493113004694.

S. Amin Yavari, S.M. Ahmadi, R. Wauthle, B. Pouran, J. Schrooten, H. Weinans, and A.A. Zadpoor. Relationship between unit cell type and porosity and the fatigue behavior of selective laser melted meta-biomaterials. *Journal of the Mechanical Behavior of Biomedical Materials*, 43:91 – 100, 2015. ISSN 1751-6161. doi: https://doi.org/10.1016/j.jmbbm.2014.12.015. URL http://www.sciencedirect.com/science/article/pii/S1751616114003944.

Amir A. Zadpoor. Mechanics of additively manufactured biomaterials. *Journal of the Mechanical Behavior of Biomedical Materials*, 70:1 – 6, 2017. ISSN 1751-6161. doi: https://doi.org/10.1016/j.jmbbm.2017.03.018. URL http://www.sciencedirect.com/science/article/pii/S1751616117301303. Mechanics of additively manufactured biomaterials and implants.

Amir A. Zadpoor. Mechanical performance of additively manufactured meta-biomaterials. *Acta Biomaterialia*, 85:41 – 59, 2019. ISSN 1742-7061. doi: https://doi.org/10.1016/j.actbio.2018.12.038. URL http://www.sciencedirect.com/science/article/pii/S1742706118307633.

A. Zargarian, M. Esfahanian, J. Kadkhodapour, and S. Ziaei-Rad. Numerical simulation of the fatigue behavior of additive manufactured titanium porous lattice structures. *Materials Science and Engineering: C*, 60: 339 – 347, 2016. ISSN 0928-4931. doi: https://doi.org/10.1016/j.msec.2015.11.054. URL http://www.sciencedirect.com/science/article/pii/S0928493115305853.

Appendix A

Data Sheet Epoxy

3M™ Scotch-Weld™ EC-9323 B/A

Two Part Structural Adhesive

Product Description

3M™ Scotch-Weld™ Structural Epoxy Adhesive EC-9323 B/A is a two component epoxy paste adhesive which cures at room temperature or with mild heat to form a tough, impact resistant structural bond. It has an excellent adhesion to a wide variety of substrates such as metals, glass, ceramics and plastics, incl. GFRP and CFRP. Once cured it provides extremely high shear and peel strength over a wide temperature range, with outstanding resistance to harsh environments and chemicals commonly encountered in aerospace applications.

Key Features

- Toughened system providing extremely high shear and peel strength
- Wide service temperature range
- Outstanding environmental resistance
- Full room temperature processing

Product Characterization

The following technical information and data should be considered representative or typical only and should not be used for specification purpose

General Properties	Part B	Part A
Colour	Off-white	Red-orange
Base	Modified epoxy	Modified amine
Consistency	Thixotropic paste	Slight gel
Density	1.18 g / cm³	1.06 g / cm³
Solids	100 %	100 %
Viscosity [a]	700 Pas	18 Pas
Mix ratio by weight (by volume)	100 : 27 wt. (100 : 30 vol.)	
Work life [b] / Open Time at 23 ± 2 °C	150 minutes / 20 minutes	
Strength build-up at 23 ± 2 °C	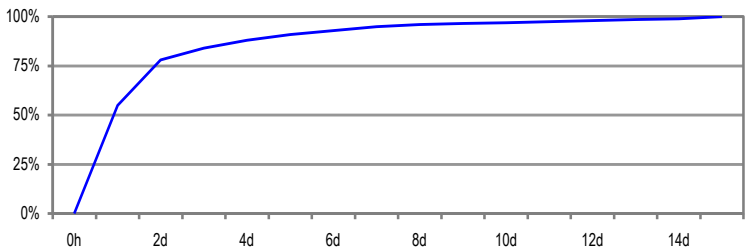	
Handling strength[c]	4-5 hours	
Full cure cycle	14 days at room temperature	
Packaging	Cans and pails	

[a] Brookfield RVF Spindle 7, 2 rpm *[b] 50 g of mixed adhesive* *[c] Time to reach 1 MPa Overlap Shear Strength*

Product Performance

The following data show typical values obtained with Scotch-Weld™ EC-9323 B/A on unprimed, sulfochromic etched, 2024 T3 aluminium. The samples have been cured for 15 days at room temperature, if not stated otherwise. To control the bond line thickness, approximately 1 wt. % of glass beads, 90 – 150 µm diameter were added to the adhesive.

Mechanical Properties		Test Temperature	Cured for 15 days at 23 °C	Cured for 2 hours at 65 °C
Overlap Shear Strength EN 2243-1		-55 °C	38 MPa	42 MPa
		23 °C	36 MPa	40 MPa
		80 °C	22 MPa	22 MPa
		120 °C	4 MPa	4 MPa
		150 °C	2 MPa	-
Overlap Shear Strength EN 2243-1	Stainless steel	23 °C	-	27 MPa
	CFRP, GFRP epoxy matrix resin	23 °C	-	28 MPa [(d)]
	PMMA	23 °C	-	3 MPa [(d)]
Floating Roller Peel Strength EN 2243-2		-55 °C	120 N / 25 mm	90 N / 25 mm
		23 °C	170 N / 25 mm	190 N / 25 mm
		80 °C	145 N / 25 mm	145 N / 25 mm
Impact Resistance ANFOR NF 76-115		23 °C	17,4 kJ / m²	32,2 kJ / m²

[(d)] Substrate Failure

Environmental Ageing

The following data show typical values obtained with Scotch-Weld™ EC-9323 B/A after 750 hours exposure to different media and environments to determine the aging resistance. The samples have been cured for 15 days at room temperature.

Mechanical Properties	Environment	Test Temperature	Results
Overlap Shear Strength EN 2243-1	Demineralized water at 23 ± 2 °C	23 °C	34 MPa
	Gasoline super at 23 ± 2 °C	23 °C	36 MPa
	Engine oil (20W40) 23 ± 2 °C	23 °C	36 MPa
	Hydraulic fluid skydrol 500B at 23 ± 2 °C	23 °C	37 MPa
	JP4 fluid at 23 ± 2 °C	23 °C	36 MPa
	5 % Salt spray at 23 ± 2 °C	23 °C	34 MPa
	Hot / Wet 70 °C, ≥ 95% R.H.	23 °C	33 MPa
	Dry heat at 120 ± 2 °C	23 °C	35 MPa

3M™ Scotch-Weld™ Structural Epoxy Adhesive EC-9323-150 B/A

Scotch-Weld™ EC-9323-150 B/A is a product modification of Scotch-Weld™ EC-9323 B/A. There are no significant differences in terms of performance. It contains 1 wt % of glass beads 90 – 150 µm diameter for bond line thickness control. Slight differences can be observed in density and viscosity.

Handling, Application, Storage

Precautionary Information

Refer to product label and Material Safety Data Sheet (MSDS) for health and safety information before using this product. For MSDS visit our website www.3M.com/msds.

Instructions for use

While this information is provided as general application guideline based upon typical conditions, it is recognized that no two applications are identical due to, among other things, differing assemblies, methods of heat and pressure application, production equipment and other limitations. It is therefore suggested that experiments be run, within the actual constrains imposed to determine optimum conditions for your specific application and to determine suitability of product for particular intended use.

Process step	Instruction
Surface preparation	The strength and durability of a bonded joint are dependent on proper treatment of the surface to be bonded. An acclimated, thoroughly cleaned, dry, grease-free surface is essential for maximum performance. Cleaning methods which will produce a break free water film on metal surfaces are generally satisfactory. At the very least, joint surfaces should be cleaned with a good proprietary degreasing agent and mechanically abraded, e.g. with 3M Scotch-Brite™ 7447. Abrading should be followed by a second degreasing treatment, e.g. with 3M 08984 Adhesive Cleaner. Optimum processing temperature for substrates and adhesive is around room temperature of 23 °C.
Application	This product consists of two parts. Combine Part B and Part A in a separate container just prior to application in the proportions specified. **Note**: Mix ratio deviations above +/- 5 % have significant influence on material performance. Mix both components thoroughly until a uniform colour is obtained. **Important:** Be careful when mixing quantities larger than 100 grams, because exothermic reaction may occur. Apply adhesive to parts to be bonded before the work life expires, e.g. by spatula. **Note:** Work life depends to some extent on mixed quantity and the shape of the container. Use of a shallow container will minimize the quantity impact. In order to obtain optimum mechanical performance, the joint components should be assembled and clamped as soon as the adhesive has been applied and before end of the open time. A fixation of the joint and an even contact pressure throughout the joint area during cure will ensure optimum performance. Maximum shear strength is obtained with 0.10 – 0.20 mm bond line thickness. Close the containers after use to protect the material against humidity.
Curing	Once mixed, Scotch-Weld™ EC-9323 B/A will gel in 3 hours, build up handling strength in 4-5 hours and fully cure within 14 days at room temperature. **Note:** Lower temperature will slow down the reaction times. Curing time can be accelerated by mild heat. Following times and temperatures will result in a full cure: ▪ 14 days at 23 ± 2 °C ▪ 2 hours at 65 ± 2 °C ▪ 15 minutes at 100 ± 2 °C **Note:** The curing temperature may have influence on the final product performance.
Cleaning	Excess uncured adhesive can be cleaned with ketone type solvents. After cure the adhesive can be removed mechanically. **Note**: When using solvents, extinguish all ignition sources, including pilot lights, and follow the manufacturer's precautions and instructions for use.
Storage and Handling	Store the product at room temperature. Shelf life is minimum 12 months from date of shipment in the original unopened containers. The specific expiry date is mentioned on the product label.

Automotive and Aerospace Solutions Division
European Aerospace Laboratory
www.3m.eu/aerospace

Reference: 222

Appendix B

Material Data Ti-6Al-4V Powder

RENISHAW
apply innovation™

Ti6Al4V ELI-0406 powder for additive manufacturing

Process specification

Powder description	Titanium alloy powder
Layer thickness	30 µm and 60 µm
Laser power	200 W
Additive manufacturing system	AM250

Material description

Ti6Al4V ELI-0406 alloy comprises titanium mass fraction up to 90% alloyed with aluminium up to 6.75% and vanadium up to 4.5%, along with other minor elements. Ti6Al4V grade 23 is otherwise referred to as Extra Low Interstitial (ELI) with regards to the interstitial impurities oxygen, carbon, and nitrogen. It is a higher purity version of the most commonly used titanium alloy Ti6Al4V grade 5. The reduced interstitial elements in grade 23 lead to an increase in both ductility and fracture toughness.

Ti6Al4V ELI-0406 has excellent specific strength (strength to weight ratio) which makes it an ideal choice where weight saving load structures are required. It has good corrosion resistance, it is also biocompatible, so can be used for a range of surgical and dental applications. For medical and dental applications Renishaw supplies Ti DG1 powder, for more infomation refer to document H-5983-9026.

Material properties

- High specific strength
- High corrosion resistance
- Excellent biocompatibility
- Good osseointegration
- Low thermal expansion
- Low thermal conductivity

Applications

- Medical and dental (Refer to document H-5983-9026)
- Aerospace and defence
- Motor sport
- Jewellery and art
- Maritime applications
- High-end sports equipment

Generic data - wrought material

Density	4.42 g/cm^3
Thermal conductivity	6 W/mK to 8 W/mK
Melting range	1635 °C to 1665 °C
Coefficient of thermal expansion (see note 1)	8 × 10^{-6} K^{-1} to 9 × 10^{-6} K^{-1}

Note 1 In the range of 0 °C to 100 °C.

Note 2 Annealed at 850 °C ±10 °C for 2 hr.

Note 3 Tested at ambient temperature to ASTM E8. Machined before testing. Values based on a sample size of 6.

Note 4 Tested to ASTM E384-11, after polishing.

Note 5 Tested to JIS B 0601-2001 (ISO 97), after bead blasting.

Note 6 HIP (hot isostatic pressing).

Composition of powder

Element	Mass (%)
Titanium	Balance
Aluminium	5.50 to 6.50
Vanadium	3.50 to 4.50
Iron	≤ 0.25
Oxygen	≤ 0.13
Carbon	≤ 0.08
Nitrogen	≤ 0.05
Hydrogen	≤ 0.012
Yttrium	≤ 0.005
Residuals	≤ 0.10 each, ≤ 0.40 total

*ASTM standard composition powder. Renishaw powders are supplied to a tighter specification to minimise batch-to-batch variations. Results quoted in this data sheet are from samples produced using Renishaw's tighter specification powder. Please contact Renishaw for further information about specifications or if you require support in qualifying non-Renishaw powders.

Mechanical properties of additively manufactured components processed in 30 µm layers

	Heat treated (See note 2)		**HIP treated** (see note 6)	
	Mean	**Standard deviation (±1σ)**	**Mean**	**Standard deviation (±1σ)**
Ultimate tensile strength (UTS) (See note 3)				
Horizontal direction (XY)	1089 MPa	7 MPa	1033 MPa	4 MPa
Vertical direction (Z)	1085 MPa	12 MPa	1034 MPa	7 MPa
Yield strength (see note 3)				
Horizontal direction (XY)	1007 MPa	5 MPa	947 MPa	4 MPa
Vertical direction (Z)	985 MPa	23 MPa	923 MPa	21 MPa
Elongation at break (See note 3)				
Horizontal direction (XY)	16%	1%	16%	1%
Vertical direction (Z)	14%	1%	17%	1%
Modulus of elasticity (see note 3)				
Horizontal direction (XY)	129 GPa	7 GPa	127 GPa	3 GPa
Vertical direction (Z)	126 GPa	15 GPa	125 GPa	4 GPa
Hardness (Vickers) (see note 4)				
Horizontal direction (XY)	368 HV0.5	10 HV0.5	352 HV0.5	9 HV0.5
Vertical direction (Z)	372 HV0.5	7 HV0.5	360 HV0.5	7 HV0.5
Surface roughness (R_a) (See note 5)				
Horizontal direction (XY)	4 µm to 6 µm			
Vertical direction (Z)	4 µm to 7 µm			

Density of additively manufactured Ti6Al4V is typically 99.8%, measured optically on a 10 mm × 10 mm × 10 mm sample at 75× magnification.

Renishaw plc
Stone Business Park
Brooms Road, Stone
Staffordshire, ST15 0SH
United Kingdom

T +44 (0)1785 285000
F +44 (0)1785 285001
E uk@renishaw.com

www.renishaw.com

RENISHAW
apply innovation™

Mechanical properties of additively manufactured components processed in 60 µm layers

	Heat treated (see note 2)		**HIP treated** (see note 6)	
	Mean	**Standard deviation (±1σ)**	**Mean**	**Standard deviation (±1σ)**
Ultimate tensile strength (UTS) (see note 3)				
Horizontal direction (XY)	1091 MPa	6 MPa	1052 MPa	3 MPa
Vertical direction (Z)	1084 MPa	8 MPa	1058 MPa	9 MPa
Yield strength (see note 3)				
Horizontal direction (XY)	1020 MPa	25 MPa	957 MPa	2 MPa
Vertical direction (Z)	987 MPa	22 MPa	973 MPa	24 MPa
Elongation at break (see note 3)				
Horizontal direction (XY)	16%	1%	16%	1%
Vertical direction (Z)	17%	1%	18%	1%
Modulus of elasticity (see note 3)				
Horizontal direction (XY)	132 GPa	9 GPa	127 GPa	3 GPa
Vertical direction (Z)	128 GPa	7 GPa	131 GPa	6 GPa
Hardness (Vickers) (see note 4)				
Horizontal direction (XY)	363 HV0.5	11 HV0.5	361 HV0.5	7 HV0.5
Vertical direction (Z)	363 HV0.5	13 HV0.5	360 HV0.5	10 HV0.5
Surface roughness (R_a) (see note 5)				
Horizontal direction (XY)	3 µm to 4 µm			
Vertical direction (Z)	5 µm to 7 µm			

Density of additively manufactured Ti6Al4V is typically 99.8%, measured optically on a 10 mm × 10 mm × 10 mm sample at 75× magnification.

For worldwide contact details, please visit www.renishaw.com/contact

Issued: 06.2017

H-5800-1086-04-C

Appendix C

Camera Specifications

EO USB 3.0 CMOS MACHINE VISION CAMERAS

- **Compact Designs for Maximum Flexibility**
- **USB 3.0 Interface for Maximum Data Transfer Speed**
- **Lightweight Housing**

EO USB 3.0 CMOS Machine Vision Cameras are lightweight, compact solutions for a range of machine vision applications. Available in 0.4 - 18.1 MegaPixel options, these cameras utilize USB 3.0 interfaces for maximum data transfer speeds of up to 5Gbits/s. EO USB 3.0 CMOS Machine Vision Cameras feature GPIO trigger/flash and lockable micro USB 3.0 connectors to ensure durability and consistency. **Note:** USB 3.0 cable (sold separately) required for operation.

Type of Sensor:	Progressive Scan CMOS
Dimensions (mm):	29 x 29 x 29 (LE: 47 x 46 x 28)
Weight (g):	52 (LE:41)
Video Output:	USB 3.0
Synchronization:	Internal or Via Software
Mount:	C-Mount (LE: C/CS-Mount)

Visit www.edmundoptics.com/3519 for additional models and accessories

EO USB 3.0 CMOS MACHINE VISION CAMERAS

Model Number:	EO-1312	EO-2323	EO-23121	EO-32121	EO-32122	N EO-4010	EO-50232	EO-5310	EO-6412
Item Number:	UI-3240	UI-3160	UI-3060	UI-3070	UI-3270	UI-3370	UI-3280	UI-3180	UI-3880
Imaging Device:	e2v EV76C560ABT/CT	ON Semi PYTHON 2000	Sony IMX174	Sony IMX252	Sony IMX265	CMOSIS CMV4000	Sony IMX264	ON Semi PYTHON 5000	Sony IMX178
Camera Sensor Format:	1/1.8"	2/3"	1/1.2"	1/1.8"	1/1.8"	1"	2/3"	1"	1/1.8"
Sensing Area, H x V (mm):	6.79 x 5.43	9.22 x 5.76	11.3 x 7.1	7.09 x 5.32	7.09 x 5.32	11.26 x 11.26	8.45 x 7.07	12.44 x 9.83	7.41 x 4.98
Pixels (H x V):	1280 x 1024	1920 x 1200	1920 x 1200	2056 x 1542	2056 x 1542	2048 x 2048	2456 x 2054	2592 x 2048	3088 x 2076
Pixel Size, H x V (µm):	5.3 x 5.3	4.8 x 4.8	5.86 x 5.86	3.45 x 3.45	3.45 x 3.45	5.5 x 5.5	3.45 x 3.45	4.8 x 4.8	2.4 x 2.4
Frame Rate (fps):	60	180	161	134	57	80	36	81	58.7
Shutter:	Global or Rolling	Global	Global	Global	Global	Global	Global	Global	Rolling
Monochrome Camera N	#37-553 $850.00	#34-849 $875.00	#33-524 $925.00	#37-314 $1,095.00	#37-316 $750.00	#37-547 $2,095.00	#34-855 $1,360.00	#34-851 $1,250.00	#37-312 $725.00
Color Camera N	#37-552 $850.00	#34-850 $875.00	#33-525 $925.00	#37-315 $1,095.00	#37-317 $750.00	#37-546 $2,095.00	#34-856 $1,360.00	#34-852 $1,250.00	#37-313 $725.00
NIR Camera	#37-327 $895.00	N/A –	N/A –	N/A –	N/A –	#37-325 $2,995.00	N/A –	N/A –	N/A –
Lite Edition Monochrome	#89-733 $575.00	N/A –	N/A –	N/A –	N/A –	N/A –	N/A –	N/A –	N/A –
Lite Edition Color	#89-734 $575.00	N/A –	N/A –	N/A –	N/A –	N/A –	N/A –	N/A –	N/A –

EO USB 3.1 CMOS MACHINE VISION CAMERAS

- **USB 3.1 = Higher Transfer Rates up to 5 Gbps**
- **Features a Reversible USB Type-C Connector**
- **Compact Housing: 47 x 46 x 26.3mm**

EO USB 3.1 CMOS Machine Vision Cameras provide high transfer rates up to 5 Gbps by utilizing a reversible Type-C USB connector. These cameras feature a compact size and two M3 screw holes on the underside of the camera to provide easy attachment to the ¼-20 mounting adapter. The camera software is easy to use and offers a wide range of driver libraries for ActiveX, DirectShow, TWAIN, LabVIEW™, and more. EO USB 3.1 CMOS Machine Vision Cameras offer quick, simple, plug and play integration, making them the ideal cost-effective camera for OEM applications.

Visit www.edmundoptics.com/3844 for additional models and compatible accessories

EO USB 3.1 CMOS MACHINE VISION CAMERAS

Model Number:	EO-0514	EO-2113	EO-3212	EO-6412
Item Number:	UI-3130LE	UI-3860LE	UI-3270LE	UI-3880LE
Imaging Device:	ON Semi PYTHON 480	Sony IMX290	Sony IMX265	Sony IMX178
Camera Sensor Format:	¼"	⅓"	1/1.8"	1/1.8"
Sensing Area, H x V (mm):	3.9 x 2.9	5.6 x 3.2	7.1 x 5.3	7.4 x 5.0
Pixels (H x V):	808 x 608	1936 x 1096	2056 x 1542	3088 x 2076
Pixel Size, H x V (µm):	4.8 x 4.8	2.9 x 2.9	3.45 x 3.45	2.4 x 2.4
Frame Rate (fps):	135	135	57	58.7
Shutter:	Global	Rolling	Global	Rolling
Mount:	C/CS-Mount	C/CS-Mount	C/CS-Mount	C/CS-Mount
Monochrome Camera	#37-333 $395.00	#37-335 $495.00	#37-337 $650.00	#37-339 $550.00
Color Camera	#37-334 $395.00	#37-336 $495.00	#37-338 $650.00	#37-340 $550.00

N NEW PRODUCT NEW LOW PRICE

Appendix D

Lens Specifications

TECHSPEC® GOLD SERIES FOCUSABLE TELECENTRIC LENS

#55-349 • 161 – 186mm WD • 0.25X

Important tools for machine vision systems and metrology applications, TECHSPEC® Gold Series Focusable Telecentric Lenses yield images from which precise measurements can be taken. These lenses yield constant magnification over a defined depth of field and are optimized to provide <0.2° telecentricity when used in the specified working distance range. Anywhere within the specified working distance, the same magnification can be obtained simply by refocusing. Both the aperture and focusing adjustment positions can be fixed by set screws to remain secure in high vibration environments.

Primary Magnification:	0.25X
Working Distance[1]:	161 - 186mm
Depth of Field[2]:	±8.2mm at f10 (20% @ 20 lp/mm)
Length:	196.3mm
Filter Thread:	M72 x 0.75
Max. Sensor Format:	⅔"
Camera Mount:	C-Mount

Telecentricity:	<0.1°
Distortion:	<0.5%
Resolution[2]:	>55% @ 40 lp/mm
Aperture (f/#):	f/6 - f/25, lockable
Object Space NA:	0.021
Number of Elements (Groups):	10 (7)
AR Coating:	425 - 675nm BBAR
Weight:	1.44kg

Sensor Size	¼"	⅓"	½.5"	½"	⅓.8"	⅔"	1"	4⁄3"
Field of View[3]	14.4mm	19.2mm	22.8mm	25.6mm	28.7mm	35.2mm	N/A	N/A

1. From front of housing 2. Image space MTF contrast 3. Horizontal FOV on standard 4:3 sensor format

Specifications subject to change

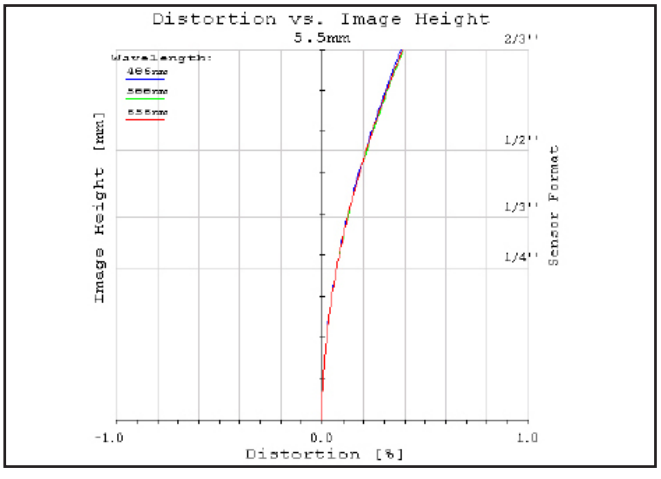

Figure 1: Distortion at the maximum sensor format. Positive values correspond to pincushion distortion, negative values correspond to barrel distortion.

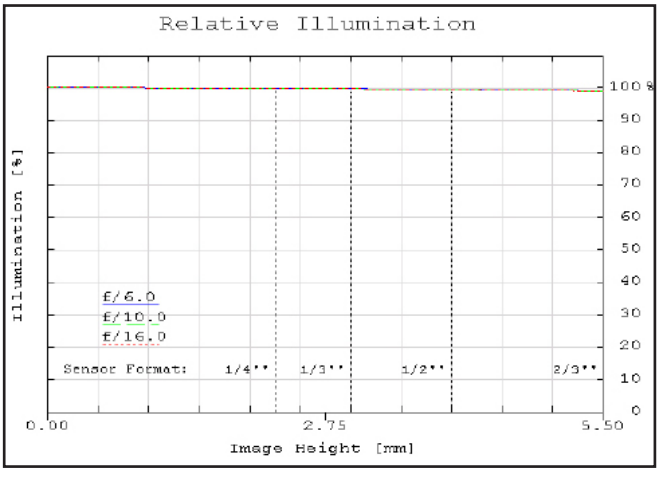

Figure 2: Relative illumination (center to corner)

In both plots, field points corresponding to the image circle of common sensor formats are included. Plots represent theoretical values from lens design software. Actual lens performance varies due to manufacturing tolerances.

TECHSPEC® GOLD SERIES FOCUSABLE TELECENTRIC LENS

#55-349 • 161 – 186mm WD • 0.25X

MTF & DOF: f/6.0

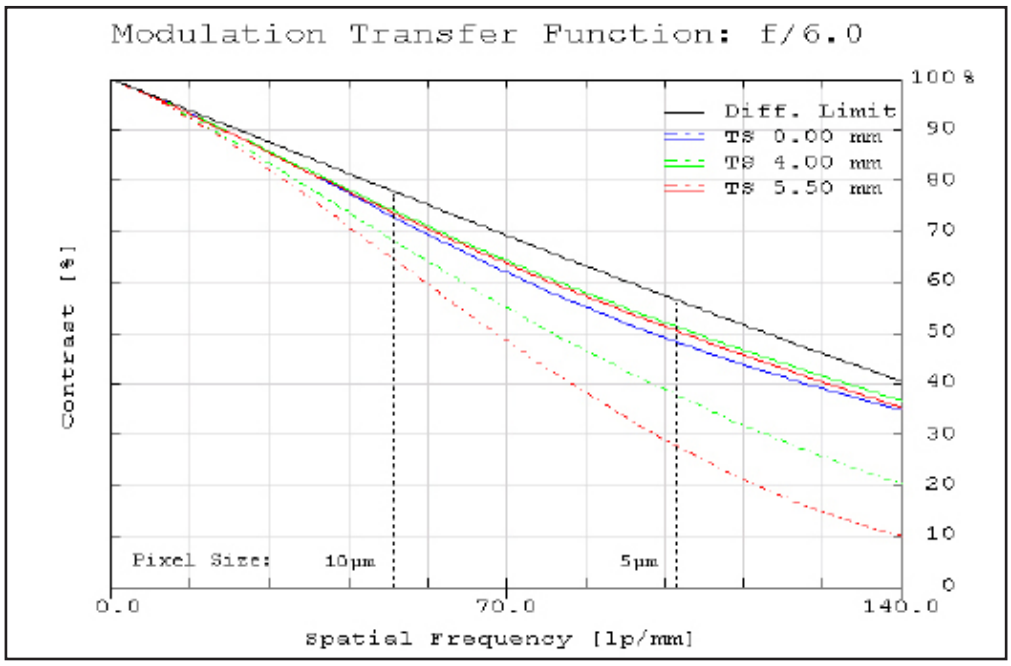

Figure 3: Image space polychromatic diffraction FFT Modulation Transfer Function (MTF) for λ = 486nm to 656nm. Included are Tangential and Sagittal values for field points on center, at 70% of full field and at the maximum sensor format. Solid black line indicates diffraction limit determined by f/#-defined aperture. Frequencies corresponding to the Nyquist resolution limit of pixel sizes are indicated.

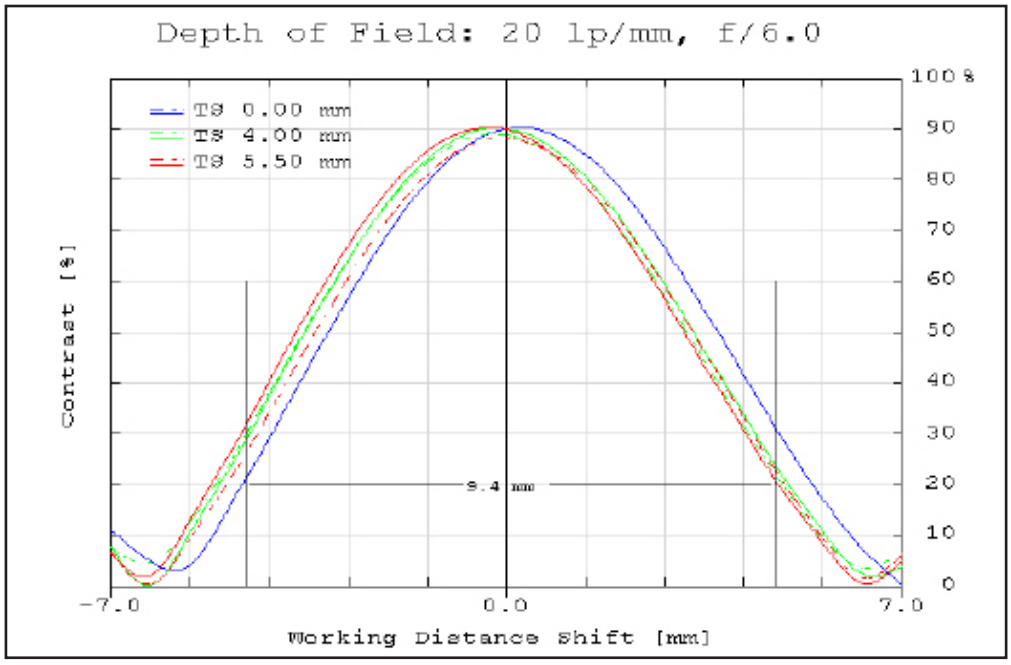

Figure 4: Polychromatic diffraction through-focus MTF at 20 linepairs/mm (image space). The depth of field at the maximum sensor format for the plotted frequency and f/# at 20% contrast is indicated by the measurement bars.

Plots represent theoretical values from lens design software. Actual lens performance varies due to manufacturing tolerances.

TECHSPEC® GOLD SERIES FOCUSABLE TELECENTRIC LENS

#55-349 • 161 – 186mm WD • 0.25X

MTF & DOF: f/10.0

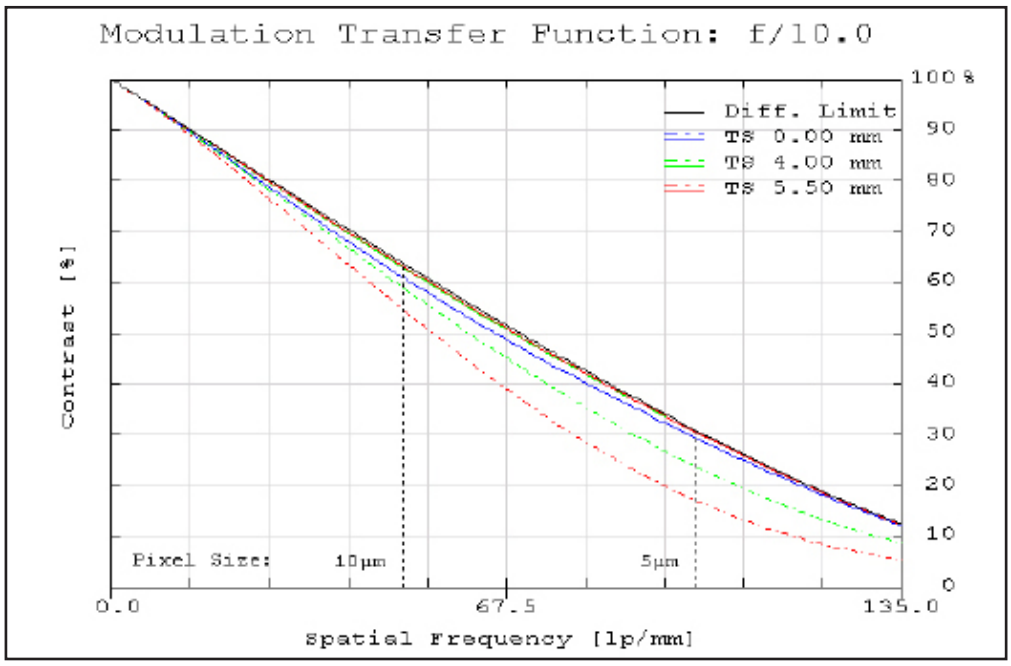

Figure 5: Image space polychromatic diffraction FFT Modulation Transfer Function (MTF) for λ = 486nm to 656nm. Included are Tangential and Sagittal values for field points on center, at 70% of full field and at the maximum sensor format. Solid black line indicates diffraction limit determined by f/#-defined aperture. Frequencies corresponding to the Nyquist resolution limit of pixel sizes are indicated.

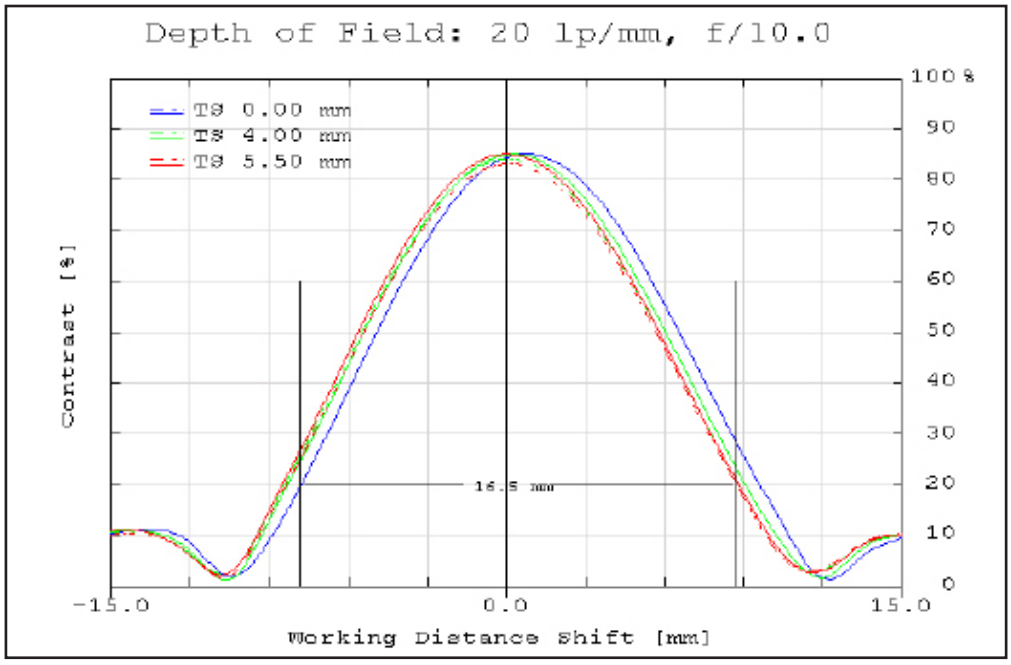

Figure 6: Polychromatic diffraction through-focus MTF at 20 linepairs/mm (image space). The depth of field at the maximum sensor format for the plotted frequency and f/# at 20% contrast is indicated by the measurement bars.

Plots represent theoretical values from lens design software. Actual lens performance varies due to manufacturing tolerances.

Eidgenössische Technische Hochschule Zürich
Swiss Federal Institute of Technology Zurich

Declaration of originality

The signed declaration of originality is a component of every semester paper, Bachelor's thesis, Master's thesis and any other degree paper undertaken during the course of studies, including the respective electronic versions.

Lecturers may also require a declaration of originality for other written papers compiled for their courses.

I hereby confirm that I am the sole author of the written work here enclosed and that I have compiled it in my own words. Parts excepted are corrections of form and content by the supervisor.

Title of work (in block letters):

Mechanical Behaviour of Additively Manufactured Ti-6Al-4V Lattices for Biomedical Implants

Authored by (in block letters):

For papers written by groups the names of all authors are required.

Name(s):	**First name(s):**
Fürer	Mickey

With my signature I confirm that

- I have committed none of the forms of plagiarism described in the 'Citation etiquette' information sheet.
- I have documented all methods, data and processes truthfully.
- I have not manipulated any data.
- I have mentioned all persons who were significant facilitators of the work.

I am aware that the work may be screened electronically for plagiarism.

Place, date	**Signature(s)**
Zürich, 14.04.2020	

For papers written by groups the names of all authors are required. Their signatures collectively guarantee the entire content of the written paper.